JOURNAL OF PETROLOGY | VOLUME 42 | NUMBER 12 | PAGES 2231–2258 | 2001

Phase Equilibrium Constraints on Intensive Crystallization Parameters of the Ilímaussaq Complex, South Greenland

GREGOR MARKL*, MICHAEL MARKS, GREGOR SCHWINN AND HOLGER SOMMER

INSTITUT FÜR MINERALOGIE, PETROLOGIE UND GEOCHEMIE, EBERHARD-KARLS-UNIVERSITÄT, WILHELMSTRASSE 56, D-72074 TÜBINGEN, GERMANY

RECEIVED JUNE 26, 2000; REVISED TYPESCRIPT ACCEPTED MAY 31, 2001

The 1·13 Ga Ilímaussaq intrusive complex, South Greenland, is composed of various types of alkali granite and silica-undersaturated alkaline to agpaitic nepheline syenites related to three subsequently intruded magma batches. Mineral chemistry indicates continuous fractionation trends within each rock type, but with distinct differences among them. The last, peralkaline magma batch is the most fractionated in terms of $X_{Fe}^{mafic\ mineral}$*, feldspar composition and mineral assemblage. This indicates that an evolving magma chamber at depth discontinuously released more highly fractionated alkaline melts. Fluid inclusions in some sodalites record a pressure drop from 3·5 to 1 kbar indicating that crystallization started during magma ascent and continued in the high-level magma chamber. On the basis of phase equilibria and preliminary fluid inclusion data, crystallization temperature drops from >1000°C (augite syenite liquidus) to <500°C (lujavrite solidus) and silica activity decreases from ~0·8 to <0·3. An almost pure methane fluid phase at high temperatures and an almost pure aqueous fluid phase in the last crystallization stages of the agpaitic rocks indicate a strong increase in water activity. NaCl activity drops from 0·4 during magmatic sodalite crystallization to <0·01 (3 wt % NaCl*^{equiv}*) in the late magmatic aqueous fluids. Relative oxygen fugacity [ΔFMQ, where FMQ is fayalite–magnetite–quartz)] depends on silica and water activity via two solid–solid buffer reactions. It decreases during fractionation in the augite syenite from about FMQ – 1 to below FMQ – 4, but increases in the peralkaline stage. The extreme peralkaline fractionation trend appears to be governed by low water activity and low* SiO_2 *activity in the parental melt. Only then is methane a stable fluid phase during most of the crystallization history, which prevents early unmixing of an aqueous NaCl-bearing fluid phase.*

KEY WORDS: *Ilímaussaq; agpaite; intensive parameters; fractionation; peralkaline*

INTRODUCTION

The Ilímaussaq intrusive complex in the mid-Proterozoic Gardar rift province of South Greenland is for various reasons one of the most famous alkaline plutonic complexes in the world:

(1) it is the type locality of agpaitic rocks, i.e. of rocks with a molar ratio of (Na + K)/Al ⩾ 1·2 (Ussing, 1912) and with complex Na–Ti–Zr silicates (Sørensen, 1997);

(2) it is a world-famous mineral locality with >200 species and is the type locality for sodalite, arfvedsonite, eudialyte and many other minerals.

(3) the kakortokite rock type shows one of the most spectacular examples of magmatic layering.

The field relations, whole-rock geochemistry, systematic mineralogy and economic potential for various metals such as Zr, Be and U (see review by Bailey *et al.*, 1981; Sørensen, 2001) have been discussed in more than 100 contributions. Ussing (1912), Ferguson (1964), Engell (1973), Larsen (1976, 1977, 1981), Larsen & Sørensen (1987) and Sørensen & Larsen (1987) have presented a petrological framework based on field work, and on whole-rock geochemical and some mineral compositional data, which allows a qualitative understanding of the magmatic evolution of the Ilímaussaq complex. As most

*Corresponding author. Telephone: +49 7071 29 72930. Fax: +49 7071 29 3060. e-mail: markl@uni-tuebingen.de

of the Ilímaussaq rocks are cumulates, whole-rock geochemistry has its limitations. The only quantitative work using silicate phase compositions that also covers the agpaitic rocks is by Larsen (1976, 1977), which provides important and detailed constraints on pyroxene and aenigmatite compositions, as well as on crystallization temperature, and which allows comparison with the work by, for example, Parsons (1972, 1981), Stephenson (1976), Powell (1978), Stephenson & Upton (1982) and Upton *et al.* (1985) on different, mostly saturated to slightly undersaturated, but not agpaitic Gardar rocks. Karup-Møller (1978) presented a thorough review of the temperature, f_{S_2} and f_{O_2} conditions of formation of ore minerals found in Ilímaussaq, which pertain also to their host rocks. Fluid inclusion studies by Petersilie & Sørensen (1970), Konnerup-Madsen *et al.* (1979, 1985, 1988) and Konnerup-Madsen & Rose-Hansen (1984) have mainly focused on the discovery of more complex hydrocarbons in agpaitic fluid inclusions, although aqueous, NaCl-bearing fluid inclusions have also been described. Such aqueous fluid inclusions from the alkali granite (not dealt with here) in conjunction with estimates of the former overburden (Poulsen, 1964) have been used to infer a pressure of intrusion of ~1 kbar (Konnerup-Madsen & Rose-Hansen, 1984). Marks & Markl (2001) presented new data in a detailed phase equilibrium study on the augite syenite portion of the complex, which will be augmented by data for the agpaitic rocks from the present paper to allow derivation of quantitative petrological models.

Ilímaussaq is one of the best-known peralkaline complexes and may serve as a type example to understand their petrogenesis. In agpaitic rocks, both whole-rock and mineral ratios of Mg/Fe, Ca/(Na + K) and K/Na approach nil, and they are characterized by extreme enrichment of elements such as Na, Zr, Cl and F, and in normally low-abundance elements such as Li, Be, Rb, Ga, REE, Nb, Ta, Hf, Zn, Sn, U and Th (Sørensen, 1997). On the basis of these and many other features, these intrusions are among the most differentiated of all magmatic rocks. Generally, peralkaline, agpaitic rocks are thought to be derived from highly fractionated alkali basaltic or nephelinitic melts (Sørensen, 1997), but in detail, their derivation, their fractionation trend and tectonic or geochemical prerequisites for their formation are still enigmatic. Because many peralkaline rocks show distinct enrichment in F and Cl, it has been argued that volatiles are responsible for the special fractionation trend that finally leads to agpaitic rocks (Gerassimovsky & Kuznetsova, 1967; Kogarko, 1974; Kogarko & Romanchev, 1977, 1982). However, in principle, pressure, temperature, the activities of silica, water and NaCl, oxygen fugacity, cooling rate or the tectonic setting could be equally responsible for the unusual agpaitic fractionation trend. As we still lack adequate quantitative estimates of intrinsic parameters for agpaitic melts, we lack the tools to fingerprint the influence of the various parameters on the crystallization behaviour of these melts. It is the aim of this study to present new phase compositional data, to discuss them quantitatively in the context of the published petrogenetic model for the Ilímaussaq intrusion (Larsen & Sørensen, 1987) and to evaluate the importance of the various parameters during the formation of agpaitic melts in general.

GEOLOGICAL SETTING

The Ilímaussaq intrusion is part of the 1·1–1·3 Ga Gardar failed rifting province of South Greenland (Upton & Emeleus, 1987; Fig. 1). During this period, 10 major plutonic complexes of gabbroic and nepheline-bearing to quartz-saturated granitoid rocks intruded a basement consisting of early Proterozoic granites and gneisses (Emeleus & Upton, 1976), which was unconformably overlain by early Gardar basalts and sandstones of the Eriksfjord formation (Poulsen, 1964). The two intrusive complexes of Grønnedal-Ika (Emeleus, 1964) and Igaliko (Upton & Fitton, 1985) contain carbonatites, and many gabbroic dykes all over the Gardar province (some thousands of square kilometres) contain up to metre-scale anorthosite xenoliths (Bridgwater, 1967; Bridgwater & Harry, 1968). The association of basalts, gabbroic intrusions, anorthosite xenoliths and carbonatites with the pene-contemporaneous granitoid intrusive rocks has been interpreted to reflect large-scale melting processes of asthenospheric mantle. These melts (alkali basalts) were probably ponded at the crust–mantle boundary and by fractionation gave rise to massive-type anorthosites and later to alkaline or peralkaline melts in the roof region of these magma chambers (see also Larsen & Sørensen, 1987).

According to Larsen & Sørensen (1987), the Ilímaussaq igneous complex was formed by successive intrusion of three melt batches at ~3–4 km depth (1 kbar, Konnerup-Madsen & Rose-Hansen, 1984). The earliest of these three stages (stage I) is the augite syenite. It occurs both as thin shell with a thickness of a few hundred metres along the western, southern and southeastern margins of the intrusion and as a lid ~150 m thick on the stratigraphic top of the intrusion (Fig. 1). The petrology and mineral chemistry of this early rock type has been discussed in detail by Larsen (1976, 1981) and by Marks & Markl (2001). The augite syenite lid was later intruded by an alkali granite (stage II), which will not be discussed further in this paper.

In stage III, nepheline- and sodalite-bearing syenites formed. Minor volumes of pulaskite, foyaite and the so-called 'sodalite foyaite' are interpreted to have crystallized *in situ* from the roof downwards, whereas the 'naujaite'

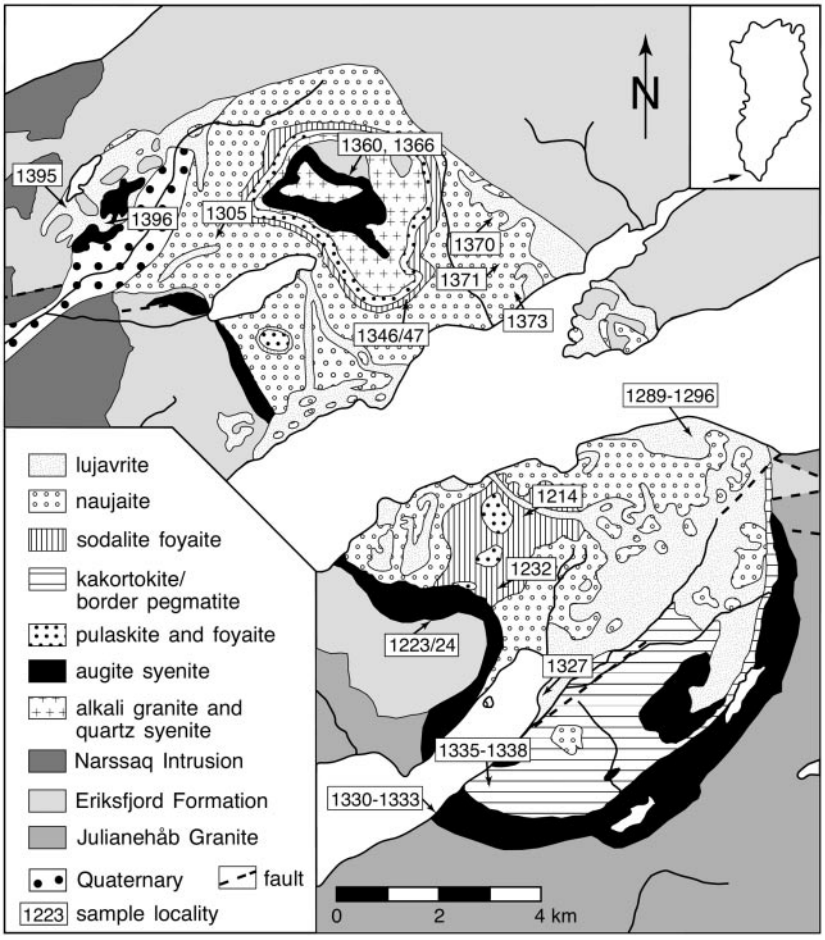

Fig. 1. Geological sketch map of the Ilímaussaq intrusion after Ferguson (1964).

represents a flotation cumulate of sodalite (Ussing, 1912; Ferguson, 1964). Mafic cumulates corresponding to this flotation cumulate are not exposed, but their existence is indicated by a strongly positive gravity anomaly beneath Ilímaussaq (Blundell, 1978; Forsberg & Rasmussen, 1978). At the top of the intrusion, the contacts between augite syenite, sodalite foyaite and naujaite appear somewhat gradational, whereas at other places, sharp cross-cutting relationships clearly demonstrate that the augite syenite is the oldest part of the intrusion. Chemically and texturally differing varieties of agpaitic nepheline syenites formed below the above-named roof rocks. The layered kakortokites crystallized at the lowermost visible stratigraphic position of the complex. The residual liquids from kakortokite crystallization formed a sequence of lujavrites, the largest masses of which occur between kakortokite and naujaite (Ferguson, 1964). Kakortokite contains xenoliths of all other rock types except for lujavrite, which also occurs as veins and irregular masses cutting through all other rock types. The rocks record extremely low viscosity of the lujavrite melt as evidenced by fluidal textures and by extreme variations in vein thickness and xenolith content over short distances.

Geochemically, typical monitors of fractionation such as Fe/Mg, Ca/(Na + K) or contents of incompatible elements indicate that later syenitic rock types in Ilímaussaq generally display higher degrees of fractionation than their precursors. The kakortokite as the only exception from this rule shows a lower Fe/Mg ratio, but on the other hand a more evolved mineral assemblage than its precursors. Eudialyte as a liquidus phase indicates that the lower Fe/Mg ratio is possibly related to contamination and does not disprove the general trend. The K/Rb ratios continuously decrease during fractionation from ~500 in the augite syenite to 35 in the most evolved lujavrites, whereas Zr/Hf and Cl/Br continuously rise from 45 to 97 and from 170 to 15 000, respectively (Bailey *et al.*, 2001). Similarly continuous trends are also exhibited by K/Cs, Sr/Ca, Li/Mg, Zn/Fe, Cs and Ga. Total rare earth element (REE) contents as well as LREE/HREE (light REE/heavy REE) ratios show a general increase with fractionation (Bailey *et al.*, 2001).

In contrast to these, more or less continously evolving fractionation indicators, elements such as Zr, Cl, F, Zn and W, show distinctive irregularities or maxima in some rock types, which are related to cumulus processes (Bailey *et al.*, 2001). A good example for this is the unusually high content of Cl in naujaite (up to 2·9 wt %) compared with the earlier (<0·2 wt %) and later (maximum 0·3 wt %) Ilímaussaq rocks.

Contamination by basalt and quartz-rich roof and sidewall rocks that occur as xenoliths in the Ilímaussaq intrusive rocks was locally shown by Ferguson (1964). On the basis of Sm–Nd data and assimilation–fractional crystallization (AFC) calculations, Stevenson *et al.* (1997) showed that the earlier Ilímaussaq rocks (augite syenite and especially the alkali granite) reflect more crustal contamination than the later agpaitic rocks.

PETROGRAPHY AND MINERAL CHEMISTRY

Petrography and mineral assemblages

Below, we briefly describe the rock types dealt with in the present paper. The mineral assemblages are listed in Table 1, and mineral abbreviations in Table 2. Detailed descriptions have been provided in many publications (e.g. Ferguson, 1964). The early magmatic and intercumulus assemblage is in some cases partially overprinted by a later magmatic assemblage and in most places by a post-magmatic or hydrothermal assemblage whose development is still related to the same magmatic event but occurs at temperatures below the solidus.

Augite syenite

The augite syenite shows a xenomorphic texture with grain size varying between 2 and 20 mm. The main liquidus mineral phases are strongly exsolved perthitic alkali feldspar, olivine, clinopyroxene and Fe–Ti oxides (Fig. 2a). In some samples, olivine is resorbed and overgrown by clinopyroxene. Most samples contain interstitial nepheline, one is quartz bearing, and some contain neither nepheline nor quartz. Biotite and amphibole may form rims around olivine, clinopyroxene or Fe–Ti oxides and are interpreted to be of near-solidus (or even subsolidus?) origin. Amphibole in most samples varies from ferropargasite to hastingsite and ferroedenite in composition. Nepheline is replaced by subsolidus assemblages consisting of analcime, sodalite, albite, muscovite and hydrogrossular (Fig. 2c and d).

Sodalite foyaite

This rock type is typically medium to coarse grained with grain sizes up to 20 mm. Early magmatic phases are exsolved euhedral perthitic alkali feldpar, nepheline, sodalite, olivine and resorbed relics of augite (Fig. 2e and i). Subsequent sector-zoned Na-rich clinopyroxene is followed by aenigmatite, fluorite, rare eudialyte and zoned ferrorichteritic, katophoritic or nyböitic amphibole, which again is partly rimmed by almost pure aegirine (Fig. 2j). In rare cases biotite overgrows early olivine. Analcime appears to occur as a late liquidus phase, but most analcime forms together with secondary sodalite by subsolidus replacement of primary sodalite and nepheline (see Fig. 2k).

Naujaite

Euhedral sodalite and nepheline are cumulate phases in this rock type (Fig. 2b). Their grain size reaches ~1 cm. Magmatic fluorite occurs as inclusions in sodalite. Alkali feldspar occurs as large tabular crystals with frequent inclusions of sodalite and is interpreted to have crystallized as the first of the interstitial minerals, which additionally comprise aegirine, arfvedsonitic to katophoritic amphibole, eudialyte and again nepheline. Subsolidus natrolite and analcime replace sodalite and feldspar, and pectolite replaces pyroxene.

Kakortokite

The kakortokite occurs as a white, a red and a black variety. The differences are caused by variations of the modal content of arfvedsonitic amphibole (black), eudialyte (red) and feldspar (white). The white and red kakortokite contain eudialyte and feldspar as early, mostly euhedral liquidus phases (Fig. 2h), whereas the black variety shows amphibole and in places pyroxene as early phases (Fig. 2g). The black and white varieties show some gravitative alignment of the tabular minerals (feldspar, amphibole). Interstitial minerals in all three varieties are sodalite and fluorite, whereas nepheline, amphibole (katophoritic to arfvedsonitic) and pyroxene are late magmatic phases depending on the type of kakortokite. The white kakortokite bears interstitial analcime, and small prismatic albite crystals in addition to aegirine pyroxene and analcime formed during hydrothermal replacement of nepheline, sodalite and early alkali feldspar.

Lujavrite

Many varieties of this rock type show flow textures. Euhedral nepheline, eudialyte, sodalite and clinopyroxene are enclosed in a mixture of albite, microcline, texturally later aegirine pyroxene, and amphibole, which are mostly aligned (Fig. 2f). Black lujavrite is distinguished from a green variety depending on the modal amount of either arfvedsonite (black) or aegirine (green).

Table 1: Mineral assemblages and fluid inclusions in the various Ilímaussaq syenites

	augite syenite	sodalite foyaite	naujaite	kakortokite	lujavrite
Early liquidus assemblages	Alkfsp + Ol + Cpx + Ap + Mnz + Bad±Timag ± Ilm±Py±Po±Plag*	Alkfsp + Cpx + Ne + Sod + Ap±Ol	Sod + Ne + Fl + Ap + Sph	Alkfsp + Eud + Ap + ... + Ne (*white*) + Ne (*red*) + Amph + Cpx (*black*)	Cpx + Amph + Eud + Ab + Mic + Sod + Ne±Steen + rare specialities (e.g. neptunite)
Interstitial phases	Ne, Qtz, Amph, Zrn	Ne, Amph, Aen, Eud	Alkfsp, Amph, Cpx, Eud, Ne	Sod, Fl ... Amph, Cpx (*white, red*), Ne, Eud (*black*)	
Near-solidus phases	Amph, Bt	Anl, Cpx, Bt	Pct, Aen	Anl, Bt	Bt, rare specialities
Subsolidus or hydrothermal phases	Sod, Anl, Ms, Hgrs, Sph, Gal, Ccp	Sod, Anl, Ab, Ntr	Ntr, Anl, Sod	Anl, Cpx, Ab	Ntr, Sod, Anl, Uss, Vil
Primary fluid inclusions	CH_4-dominated (Sod)†	CH_4-dominated (Sod)†	CH_4-dominated (Sod)	pure CH_4 (Sod)	CH_4-dominated (Ne, Fsp) and/or aqueous (Sod)
Secondary fluid inclusions			CH_4-dominated (Sod) and aqueous (Eud)	pure CH_4 (Sod)	aqueous (Sod)
Samples used in the present study	1223, 1224, 1360, 1366 and 1330–1333	1214, 1232, 1346 and 1347	1305, 1370, 1371 and 1373	1335, 1337 and 1338	1289, 1294, 1296, 1327, 1395 and 1396

*After Larsen (1981).
†After Petersilie & Sørensen (1970).

Table 2: Mineral abbreviations used in figures and text

Mineral	Abbreviation	Mineral	Abbreviation
Ab	albite	Ilm	ilmenite
Aeg	aegirine	Jd	jadeite
Aen	aenigmatite	Kfsp	K-feldspar
Alkfsp	alkali feldspar	Mag	magnetite
Amph	amphibole	Mic	microcline
An	anorthite	Mnz	monazite
Anl	analcime	Ms	muscovite
Ann	annite	Ne	nepheline
Ap	apatite	Ntr	natrolite
Arf	arfvedsonite	Ol	olivine
Bad	baddeleyite	Pct	pectolite
Bt	biotite	Po	pyrrhotite
Ccp	chalcopyrite	Py	pyrite
Cpx	clinopyroxene	Qtz	quartz
Eud	eudialyte	Sod	sodalite
Fa	fayalite	Sph	sphalerite
Fl	fluorite	Steen	steenstrupine
Fsp	feldspar	Ti-mag	titanomagnetite
Gal	galena	Uss	ussingite
Hal	halite	Vil	villiaumite
Hgrs	hydrogrossular	Zrn	zircon

In some of the samples, rare minerals such as ussingite ($NaAlSi_3O_8.NaOH$), naujakasite, steenstrupine, villiaumite occur, in some special varieties even as major constituents. Some of the so-called lujavrites are in fact fenitized host rocks [such as a murmanite-bearing variety described by, for example, Ferguson (1964)], and these are not dealt with in the present paper. Rarely, the lujavritic melt developed silicate–silicate immiscibility features described in detail elsewhere (Markl, 2001).

Mineral chemistry

Analytical techniques

Microprobe wavelength-dispersive spectometry (WDX) analyses were performed on a Cameca SX100 system at the University of Freiburg, Germany. Natural standards supplied by Cameca were used for calibration. Analytical conditions were 15 kV and 20 nA, with counting times of 20 s for all elements on the peak and 10 s on the background. Raw data were processed by procedures described by Pouchou & Pichoir (1984). Uncertainties for major elements are estimated to be about $\pm 1\%$ (relative), for minor elements about $\pm 5\%$ (relative), and detection limits are $\sim 0{\cdot}01$ wt % depending on the specific element. The composition of exsolved microperthitic feldspar was reintegrated using the scanning mode and a window of about 20 μm × 30 μm size in cases where the exsolutions were of the order of a few microns only. For coarsely exsolved feldspars, point analyses in conjunction with image analysis techniques were used. Electron microprobe analyses of minerals used in the calculations below are reported in Tables 3–6. Data for Fe–Ti oxides have been reported in detail by Marks & Markl (2001) and are therefore not repeated here. The mineral chemistry of micas and amphiboles will be the topic of a separate paper and will therefore not be discussed here.

Olivine

Olivine occurs in the augite syenite and rarely in the sodalite foyaite. In both rock types, olivine is unzoned. Some representative analyses are shown in Table 3. Composition ranges from $Fa_{71}Tp_2$ to $Fa_{94}Tp_4$ in the augite syenite and shows a good correlation between Fe and Mn contents (Fig. 3c). In contrast, the sodalite foyaite olivine composition is almost constant between $Fa_{94}Tp_6$ and $Fa_{97}Tp_3$ (Fig. 3a). CaO in both rock types varies between 0·1 and 1·8 wt %. In the sodalite foyaite, Ca shows a strong correlation with Fa content, whereas in the augite syenite it shows wide scatter without any visible systematics (Fig. 3b). Ca-rich exsolution lamellae consisting of clinopyroxene–magnetite intergrowths in some olivines from augite syenite have been described by Markl *et al.* (2001).

Pyroxene

Larsen (1976) presented electron microprobe data of clinopyroxenes from various Ilímaussaq rock types which are now augmented by our new data (Table 4). Clinopyroxene in augite syenite is a chemically zoned subcalcic augite (Marks & Markl, 2001) with Quad components typically >90% (Fig. 4). The range of X_{Fe} (after Lindsley, 1983) in all samples is between 0·34 and 0·87. Fs content increases towards the rim of a single crystal, whereas Wo component stays approximately constant between 42 and 49 mol %, depending on the sample. Acmite contents range from 2 to 15 mol %, and only in one sample (GM1223) acmite content reaches 27 mol % (Fig. 4a).

In all other rock types, pyroxene Na and Fe^{3+} contents are significantly higher than in augite syenite whereas Ca and Fe^{2+} contents decrease strongly (Fig. 4a and b). Cores of resorbed pyroxene crystals in sodalite foyaite have augitic compositions very similar to those from the

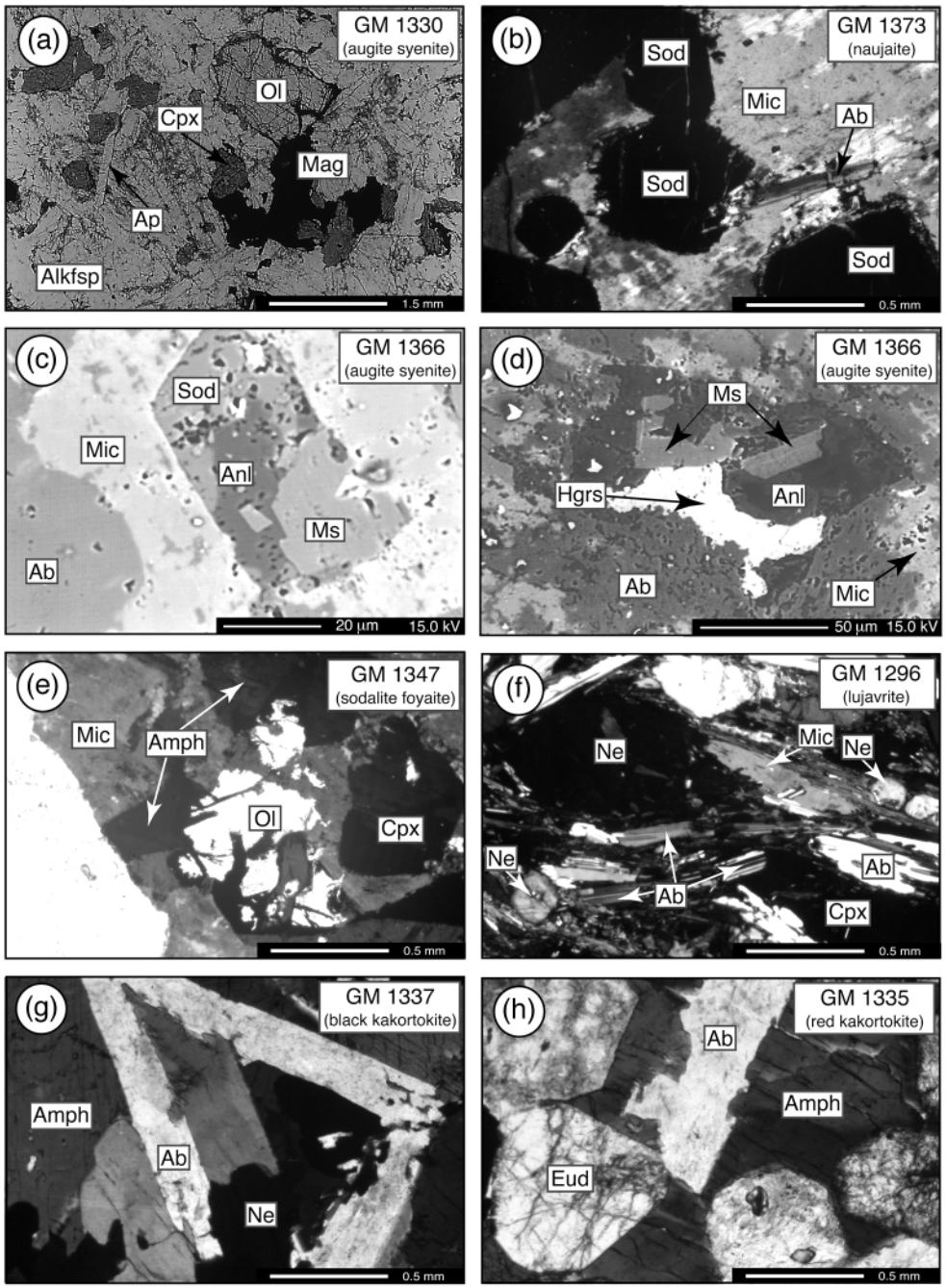

Fig. 2.

augite syenite (Fig. 4a and b). During reaction with the sodalite foyaitic melt, an aegirine pyroxene and fluorite replace the original augite (Fig. 2i). Later pyroxenes in sodalite foyaite are sector-zoned aegirine augites (Shearer & Larsen, 1994) with acmite contents up to 90 mol %. As shown in Fig. 5, zonation is mainly caused by discontinuous decrease of Fe^{2+}, Ca, Mn and Zr, whereas Na and Fe^{3+} increase. Aegirine rims around amphibole (Fig. 2j) are relatively rich in jadeite component (up to 8 mol %).

In naujaite, the pyroxene composition is almost pure aegirine with <8 mol % of Quad and <6 mol % of jadeite component. In general, the acmite component increases towards the rim of a crystal.

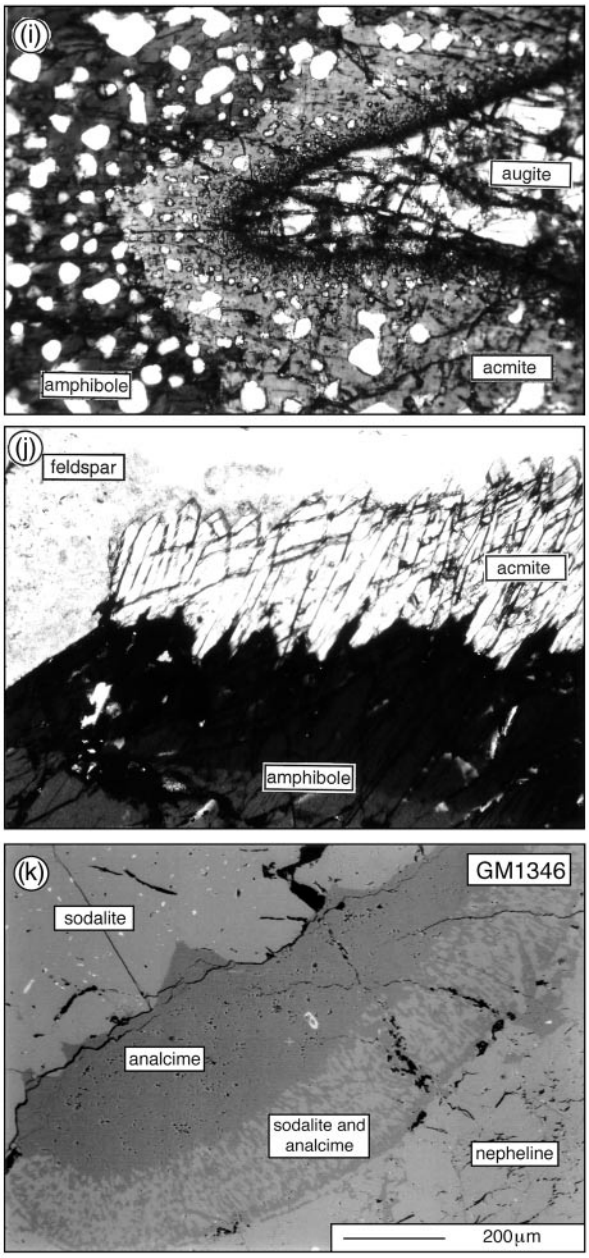

Fig. 2. Observed mineral textures in the various rock types. (a) Granular xenomorphic texture in augite syenite with olivine, clinopyroxene, Fe–Ti oxides and apatite in a matrix of alkali feldspar. (b) Euhedral sodalite crystals in exsolved alkali feldspar in naujaite. (Note the small albite inclusion.) (c) and (d) in some samples of augite syenite, nepheline is replaced by subsolidus assemblages with analcime, sodalite, albite, hydrogrossular and muscovite. (e) Olivine and clinopyroxene as inclusions in alkali feldspar from sodalite foyaite. (Note the later interstitial amphiboles.) (f) Fluidal texture in lujavrite. Large and euhedral nepheline is enclosed in a mixture of albite, microcline, aegirine pyroxene and amphibole, which are strongly aligned. (g) Black kakortokite with amphibole and feldspar as cumulus phases and nepheline as a later interstitial mineral. (h) Euhedral eudialyte and feldspar crystals together with interstitial amphibole in red kakortokite. (i) Core of augitic pyroxene in sodalite foyaite, which is resorbed and overgrown by fluorite, aegirine pyroxene and arfvedsonite. (j) Amphibole rimmed by aegirine (sodalite foyaite). (k) Symplectic intergrowth of sodalite and analcime replacing primary sodalite and nepheline in sodalite foyaite.

Pyroxenes in all types of kakortokite show the same zonation and the same exchange of Quad against acmite component as those in the sodalite foyaite, but acmite content reaches only ~75 mol %. Besides their higher Quad component, they have also a lower Fe/Mg ratio than naujaite and sodalite foyaite pyroxenes.

The clinopyroxenes in lujavrites have acmite contents >80 mol %. Four types occurring in different samples

Table 3: Representative microprobe analyses of olivine in augite syenite and sodalite foyaite

Sample:	GM1331	GM1366	GM1333	GM1214	GM1347	GM1294
Rock type:	augite syenite	augite syenite	augite syenite	sodalite foyaite	sodalite foyaite	sodalite foyaite
Mineral:	ol	ol	ol	ol	ol	ol
wt %						
SiO_2	31·22	32·02	30·03	28·99	28·50	28·77
FeO	58·64	55·05	65·68	66·11	67·07	66·17
MnO	1·94	2·20	2·85	2·87	2·63	2·87
MgO	7·94	10·46	1·60	0·23	0·18	0·24
CaO	0·21	0·17	0·53	1·18	0·77	1·13
Total	99·95	99·90	100·70	99·38	99·15	99·18
Formula based on 4 oxygens						
Si	1·00	1·00	1·00	0·99	0·99	0·99
Mg	0·38	0·49	0·08	0·01	0·01	0·01
Fe^{2+}	1·57	1·44	1·83	1·88	1·91	1·89
Mn	0·05	0·06	0·08	0·08	0·08	0·08
Ca	0·01	0·01	0·02	0·04	0·02	0·04
Sum	3·00	3·00	3·00	3·00	3·01	3·01

can be distinguished both texturally and chemically (Fig. 6a–d). Early, relatively large tabular crystals have the lowest jadeite contents (~5 mol %). Partially aligned prismatic crystals, fully aligned prismatic crystals and anhedral aggregates together with ussingite have successively higher jadeite contents up to 19 mol % (Fig. 4a).

The Zr contents in the various Ilímaussaq pyroxenes change significantly (Larsen, 1976) and systematically, and are comparable with those of the pyroxenes described by Jones & Peckett (1980) from the Igaliko complex in the Gardar province. As shown in Fig. 7, Zr in augite syenite is low and increases towards the outermost rims of the crystals (Fig. 7a) up to ~0·9 wt % ZrO_2, and in sample GM 1223 even up to 1·5 wt % (Fig. 7b). In sodalite foyaite (Fig. 7c), pyroxenes have constant Zr contents that are higher than in the naujaite pyroxenes (Fig. 7d), where Zr is also almost constant. Absolute amounts reach 1·1 and 0·6 wt % ZrO_2, respectively. Zr in kakortokites (Fig. 7e) is comparable with that in the sodalite foyaite (~1·3 wt % ZrO_2), although the contents decrease slightly towards the rim. In lujavrite pyroxenes, Zr contents are generally low (<0·5 wt % ZrO_2) and constant, but some pyroxenes with extreme Zr-rich cores (up to 2 wt % ZrO_2) were observed (Fig. 7f). This change in zoning textures is interpreted to record the early increase and later decrease of Zr content in the melt. The decrease is mainly governed by the crystallization of the Zr silicate eudialyte and may monitor its appearance on the liquidus. A plot of Ca vs Zr (Fig. 8) reveals this systematic, but discontinuous change of Zr content with rock type and Ca content. The discontinuity may be related to the geochemical discontinuity of the three magma batches or to the lack of samples from the pulaskite and foyaite unit and from the unexposed part below the kakortokite.

Alkali feldspar

In the augite syenite, sodalite foyaite, naujaite and kakortokite, alkali feldspar shows perthitic exsolution of albite in K-feldspar (Fig. 9a and b). Recalculated magmatic compositions in sodalite foyaite ($Ab_{28–42}An_{0–1}$) and kakortokite ($Ab_{30–45}An_{0–1}$) are very similar and Ca free, whereas the augite syenite ($Ab_{40}An_6Or_{54}$–$Ab_{55}An_{12}Or_{33}$) shows strongly ternary compositions (see Fig. 9d and Table 5). Texturally late, but euhedral feldspar crystals in kakortokite are pure albite. Textures indicate that the lujavrites crystallized two separate feldspars of almost albite and K-feldspar end-member composition (Fig. 9c).

Nepheline

Nepheline compositions range from $Ne_{67}Ks_{17}Qtz_{16}$ to $Ne_{74}Ks_{11}Qtz_{15}$ in the augite syenite (Table 5). Nephelines in sodalite foyaite, naujaite and kakortokite show a wide range in SiO_2 contents. They are higher in Ks component

Table 4: Representative microprobe analyses of clinopyroxenes of the various rock types

Sample:	GM1223	GM1333	GM1232	GM1214	GM1214	GM1370	GM1338	GM1294	GM1289
Rock type:	augite syenite	augite syenite	sodalite foyaite	sodalite foyaite	sodalite foyaite	naujaite	kakortokite	lujavrite	lujavrite
Mineral:	cpx	cpx	cpx (resorbed augite)	cpx (aegirine rim)	cpx	cpx	cpx	cpx (type 1)	cpx (type 3)
wt %									
SiO_2	50·51	49·70	47·80	51·16	53·04	52·46	52·74	53·24	53·92
TiO_2	0·13	0·93	0·44	1·46	0·11	0·41	0·95	0·64	0·54
Al_2O_3	1·07	1·45	0·88	1·05	2·22	1·15	1·09	1·24	5·84
FeO	25·92	18·06	28·35	30·03	30·03	30·72	31·82	29·99	25·02
MnO	0·94	0·50	0·79	0·32	0·08	0·21	0·19	0·07	0·09
MgO	1·51	6·63	0·44	0·02	0·08	0·01	0·09	0·00	0·02
ZrO_2	1·03	0·15	0·69	0·32	0·01	0·06	0·50	0·17	0·04
CaO	14·29	21·43	17·73	4·50	0·10	2·55	2·22	0·69	0·30
Na_2O	4·56	0·73	2·11	11·19	13·64	12·53	10·44	13·87	13·66
Total	99·96	99·58	99·23	100·05	99·31	100·10	100·04	99·91	99·43
Formula based on 4 cations and 6 oxygens									
Si	1·98	1·95	1·96	1·94	1·98	1·96	2·01	1·98	2·00
Al	0·05	0·07	0·04	0·05	0·10	0·05	0·05	0·05	0·25
Ti	0·00	0·03	0·01	0·04	0·00	0·01	0·03	0·02	0·02
Fe^{3+}	0·28	0·03	0·18	0·80	0·93	0·91	0·61	0·94	0·68
Mg	0·09	0·39	0·03	0·00	0·00	0·00	0·01	0·00	0·00
Fe^{2+}	0·60	0·56	0·79	0·15	0·00	0·05	0·40	0·00	0·09
Mn	0·03	0·02	0·03	0·01	0·00	0·01	0·01	0·00	0·00
Zr	0·02	0·00	0·01	0·01	0·00	0·00	0·01	0·00	0·00
Ca	0·60	0·90	0·78	0·18	0·01	0·10	0·10	0·02	0·01
Na	0·35	0·06	0·17	0·82	0·98	0·91	0·77	0·99	0·95
Sum	4·00	4·00	4·00	4·00	4·00	4·00	4·00	4·00	4·00

than those in the other rocks (Fig. 10). Nepheline in lujavrite is significantly poorer in SiO_2. The CaO content in all rock types is invariably <1 wt %. The spread in excess silica (Fig. 10) is related to patchy compositional differences within single grains and between grains, but not to a continuous growth zonation. We interpret the patchy variations as retrograde effects related to microfractures and hydrothermal fluids.

Sodalite

Primary sodalite in sodalite foyaite, naujaite and kakortokite, and post-magmatic sodalite observed in some augite syenite samples (Fig. 2b–d) are almost pure sodalite end members with maximum SO_3 contents of ~0·5 wt % (see Fig. 11 and Table 6). Subsolidus sodalite in symplectites with analcime (Fig. 2k) in sodalite foyaite and kakortokite have SO_3 contents up to 1·3 wt %. Sodalite in the various lujavrite samples covers a wide continuous compositional range with SO_3 contents between 0·9 and 3·8 wt % (solid solutions with nosean). The villiaumite (NaF)-bearing sample GM1395 shows the largest variations and the highest SO_3 contents.

Fluid inclusions

Fluid inclusion studies by Petersilie & Sørensen (1970) and Konnerup-Madsen *et al.* (1979, 1985, 1988) have shown that methane is the most important fluid phase in equilibrium with the various peralkaline melts. Higher hydrocarbons occur in small percentages, and water is almost completely absent. According to those workers, the alkali granite contains abundant primary aqueous, highly saline fluid inclusions, whereas aqueous inclusions of variable salinity are extremely rare in most of the agpaitic rocks. Preliminary results of Schwinn (1999) and

Table 5: Representative microprobe analyses of feldspar and nepheline in Ilímaussaq rocks

Sample:	GM1331	GM1223	GM1346	GM1337	GM 1295	GM 1294	GM1330	GM1347	GM1371	GM1336	GM 1296
Rock type:	augite syenite	augite syenite	sodalite foyaite	kakortokite	lujavrite	lujavrite	augite syenite	sodalite foyaite	naujaite	kakortokite	lujavrite
Mineral:	fsp (reint.)	fsp (reint.)	fsp (reint.)	fsp (reint.)	albite	microcline	nepheline	nepheline	nepheline	nepheline	nepheline
wt %											
SiO_2	62·39	66·28	64·35	66·31	69·07	64·68	45·21	44·35	42·85	42·01	42·22
Al_2O_3	22·21	19·05	19·13	19·02	19·49	18·27	32·72	33·03	33·76	33·93	34·01
FeO	0·12	0·30	0·01	0·00	0·21	0·03	0·12	0·34	0·08	0·10	0·11
MnO	0·00	0·00	0·01	0·10	0·00	0·01	0·02	0·00	0·00	0·01	0·03
MgO	0·00	0·00	0·00	0·01	0·00	0·01	0·02	0·01	0·02	0·00	0·00
BaO	1·46	0·05	0·59	0·00	0·00	0·00	n.d.	n.d.	n.d.	n.d.	n.d.
CaO	2·06	0·01	0·28	0·01	0·00	0·01	0·63	0·00	0·00	0·00	0·01
Na_2O	6·06	6·50	4·07	5·03	11·81	0·00	16·45	16·82	16·43	16·66	16·50
K_2O	5·94	7·28	10·58	9·66	0·07	16·69	4·72	6·15	7·19	6·84	6·81
Total	100·24	99·47	99·02	100·14	100·65	99·70	99·89	100·70	100·33	99·55	99·69
Oxygens p.f.u.	8	8	8	8	8	8	32	32	32	32	32
Si	2·83	2·99	2·96	2·99	3·00	3·00	8·61	8·46	8·26	8·17	8·19
Al	1·19	1·01	1·03	1·01	1·00	1·00	7·34	7·43	7·67	7·77	7·77
Mg	0·00	0·00	0·00	0·00	0·00	0·00	0·00	0·05	0·01	0·01	0·00
Fe^{2+}	0·00	0·01	0·00	0·00	0·01	0·00	0·02	0·00	0·00	0·00	0·03
Mn	0·00	0·00	0·00	0·01	0·00	0·00	0·00	0·00	0·01	0·00	0·00
Ba	0·03	0·00	0·01	0·00	0·00	0·00	0·00	0·00	0·00	0·00	0·00
Ca	0·10	0·00	0·01	0·00	0·00	0·00	0·13	0·00	0·00	0·00	0·00
Na	0·53	0·57	0·37	0·45	0·99	0·00	6·07	6·22	6·14	6·28	6·20
K	0·34	0·42	0·62	0·53	0·00	0·99	1·15	1·50	1·77	1·70	1·68
Sum	5·02	5·00	5·00	4·99	5·00	4·99	23·32	23·66	23·86	23·93	23·87

n.d., not detected; reint., reintegrated.

Table 6: Representative microprobe analyses of sodalite, hydrogrossular, white mica and biotite

Sample:	GM1360	GM1346	GM1305	GM1337	GM1395	GM1360	GM1360	GM1333
Rock type:	augite syenite	sodalite foyaite	naujaite	kakortokite	lujavrite	augite syenite	augite syenite	augite syenite
Mineral:	sod	sod	sod	sod	sod	hgrs	white mica	bio
wt %								
SiO_2	37·18	36·87	37·02	36·51	35·86	36·49	41·10	31·81
TiO_2	n.d.	n.d.	n.d.	n.d.	n.d.	n.d.	0·00	0·03
Al_2O_3	33·05	33·93	33·88	33·69	32·63	23·54	39·26	21·36
FeO	0·03	0·00	0·00	0·05	0·02	0·30	4·09	31·79
MnO	0·10	0·08	0·23	0·20	0·07	0·00	0·16	0·40
MgO	0·01	0·00	0·00	0·05	0·00	0·00	0·15	2·05
CaO	0·04	0·07	0·01	0·00	0·00	35·88	1·14	0·03
Na_2O	23·71	24·30	24·65	24·63	25·32	0·01	1·71	0·14
K_2O	0·13	0·08	0·02	0·02	0·02	0·00	8·34	8·82
SO_3	0·03	0·05	0·12	0·12	3·66	n.d.	n.d.	n.d.
Cl	7·22	6·97	7·41	7·33	5·35	0·01	0·03	0·01
F	n.d.	n.d.	n.d.	n.d.	n.d.	n.d.	0·04	0·01
Total	101·50	102·35	103·34	102·60	102·93	96·23	96·02	96·45
Oxygens p.f.u.	25	25	25	25	25	12	11	11
Si	5·95	5·85	5·85	5·81	5·39	2·86	2·76	2·55
Al	6·24	6·34	6·31	6·32	5·78	2·17	3·11	2·02
Ti	—	—	—	—	—	—	0·00	0·00
Mg	0·00	0·00	0·00	0·01	0·00	0·00	0·02	0·24
Fe^{2+}	0·00	0·00	0·00	0·01	0·00	0·02	0·23	2·33
Mn	0·01	0·01	0·03	0·03	0·01	0·00	0·01	0·03
Ca	0·01	0·01	0·00	0·00	0·00	0·00	0·08	0·00
Na	7·36	7·47	7·55	7·60	7·37	3·01	0·22	0·02
K	0·03	0·02	0·00	0·00	0·00	0·00	0·72	0·90
SO_3	0·00	0·01	0·01	0·01	0·41	—	—	—
Cl	1·96	1·87	1·98	1·98	1·36	0·00	0·00	0·00
F	—	—	—	—	—	—	0·01	0·00
Sum	19·60	19·70	19·74	19·78	18·55	8·06	7·15	8·09

n.d., not detected.

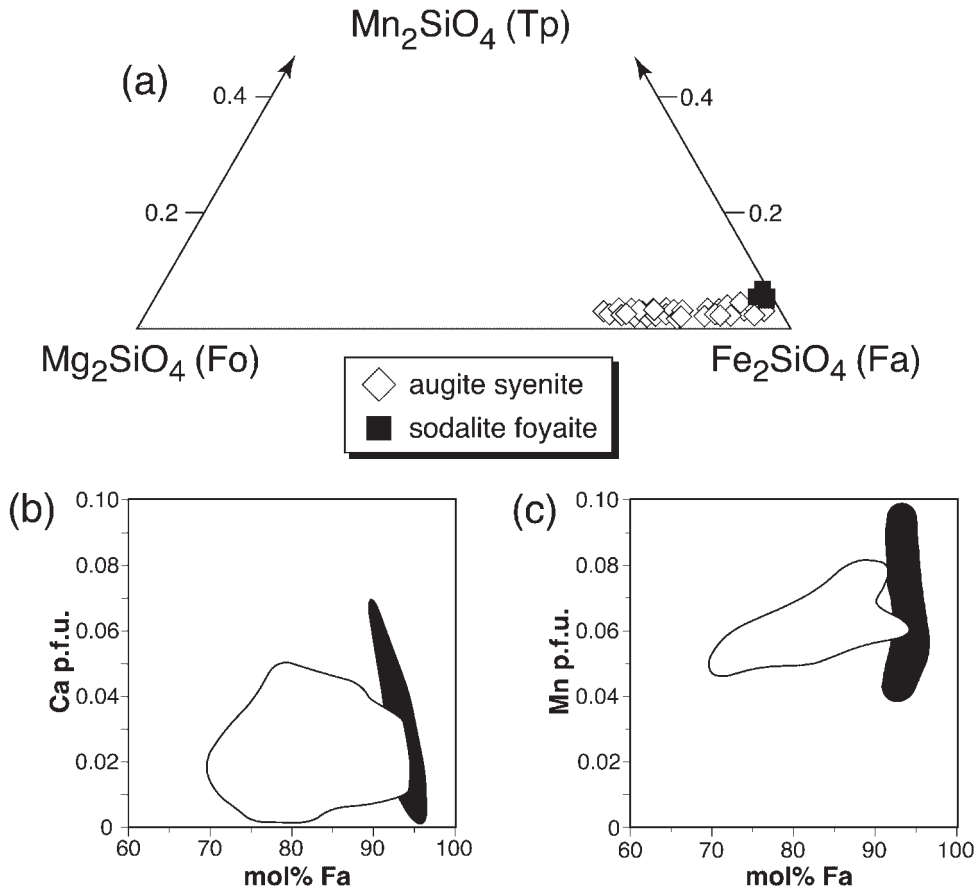

Fig. 3. (a) Fo–Fa–Tp diagram showing the Ilímaussaq olivine compositions. (b) and (c) correlation diagrams for Ca and Mn with Fa content. Here and in the following diagrams, p.f.u. stands for per formula unit.

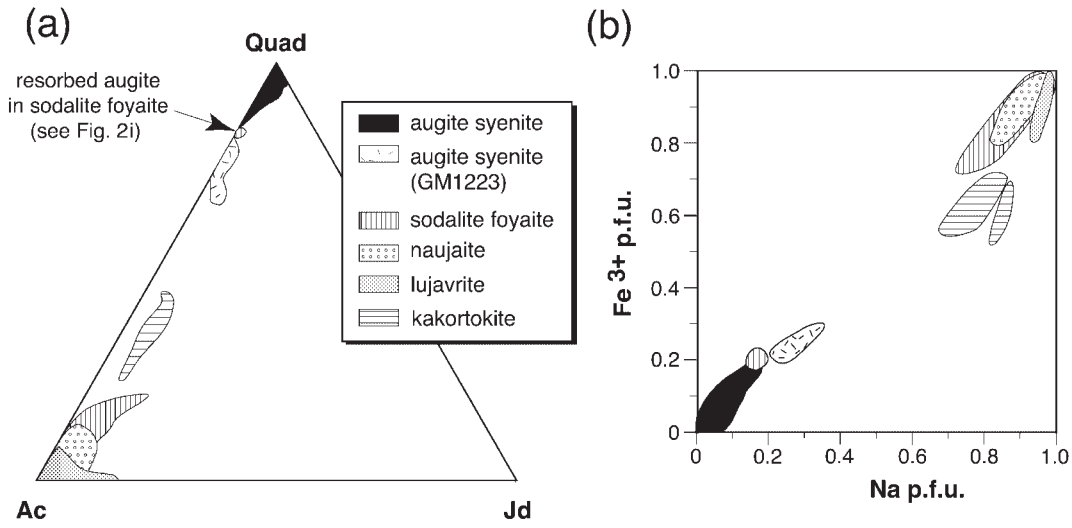

Fig. 4. (a) Pyroxene composition for the various rock types in the triangle acmite–jadeite–Quad. (b) Correlation diagram between Na and Fe^{3+} in Ilímaussaq pyroxenes.

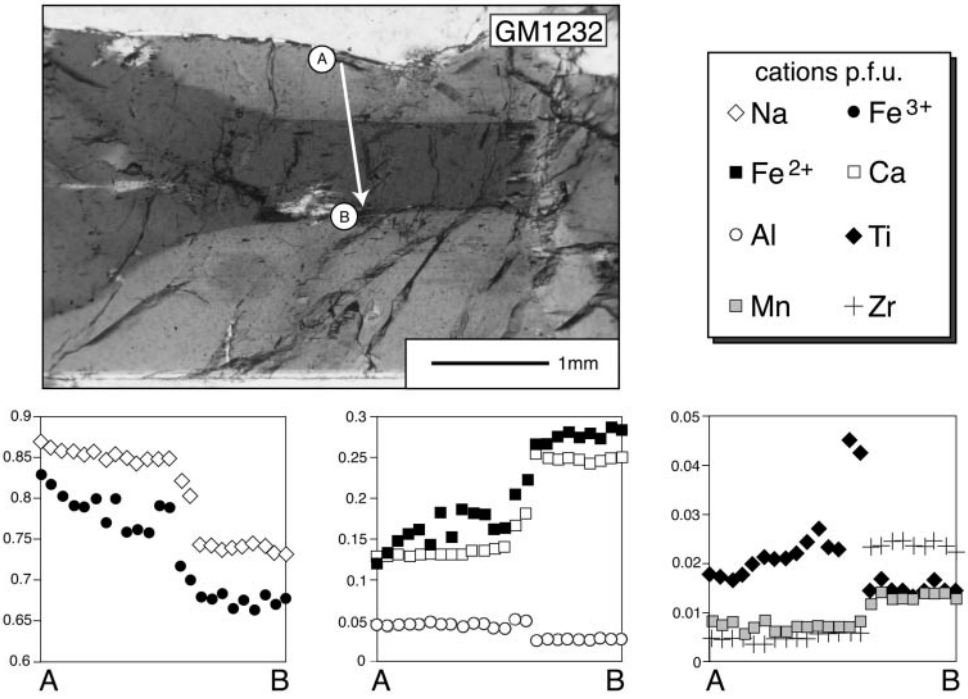

Fig. 5. Chemical variation along a profile in a sector-zoned clinopyroxene crystal from sodalite foyaite.

Sommer (1999) indicate that the primary inclusions in naujaite, kakortokite and some lujavrite samples are almost pure methane hydrocarbon inclusions, whereas some lujavrites show primary aqueous, low-salinity (~3 wt % NaCl equivalent) fluid inclusions. Secondary inclusions in the methane-bearing rocks consist of methane–water mixtures, of almost pure methane or of low-salinity aqueous fluids, whereas they comprise only aqueous, low-salinity inclusions in the investigated lujavrite samples.

PHASE EQUILIBRIA

In the different rock types, various mineral assemblages provide constraints on intensive parameters. Phase equilibria involving olivine, clinopyroxene, quartz, spinel *sensu lato* and ilmenite in the augite syenite allow the most detailed estimates concerning temperature, silica activity and oxygen fugacity (see Larsen, 1976, 1977; Marks & Markl, 2001). Additional information on this rock type and most information on the other rock types are related to equilibria in the Na–Al–Si–O–H–Cl system involving albite, jadeite, nepheline, sodalite, analcime, NaCl, SiO_2 and H_2O. The equilibria depend on pressure, temperature and some of them also on SiO_2, H_2O and/or NaCl activity. All five phases in equilibrium principally allow the calculation of four of these variables. However, as the early magmatic assemblage never involves analcime, only three parameters can be calculated for the early magmatic stages. As discussed below, pressure was fixed at 1 kbar, and hence, temperature, silica activity and NaCl activity could be calculated using the reactions

$$\mathrm{Ab} = \mathrm{Jd} + \mathrm{SiO_2} \quad (1)$$

$$\mathrm{Ab} = \mathrm{Ne} + 2\,\mathrm{SiO_2} \quad (2)$$

$$\mathrm{Ne} = \mathrm{Jd} + \mathrm{SiO_2} \quad (3)$$

and

$$3\,\mathrm{Ne} + 2\,\mathrm{NaCl} = \mathrm{Sod.} \quad (4)$$

For the calculation of end member component activities from mineral formulae, the solution models of Fuhrman & Lindsley (1988) for feldspar, Holland (1990) for clinopyroxene and Ghiorso (http://melts.geology.washington.edu) for nepheline were used. Sodalite was regarded as pure Cl end member in accordance with most of the non-lujavrite microprobe analyses. In the absence of growth zonation, we assume equilibration of the magmatic mineral assemblage as long as melt is in contact with the minerals. Accordingly, zoned clinopyroxene crystals record various stages of crystallization. For the calculation of the early magmatic crystallization conditions, we used clinopyroxene core compositions and the nepheline compositions with the highest amounts

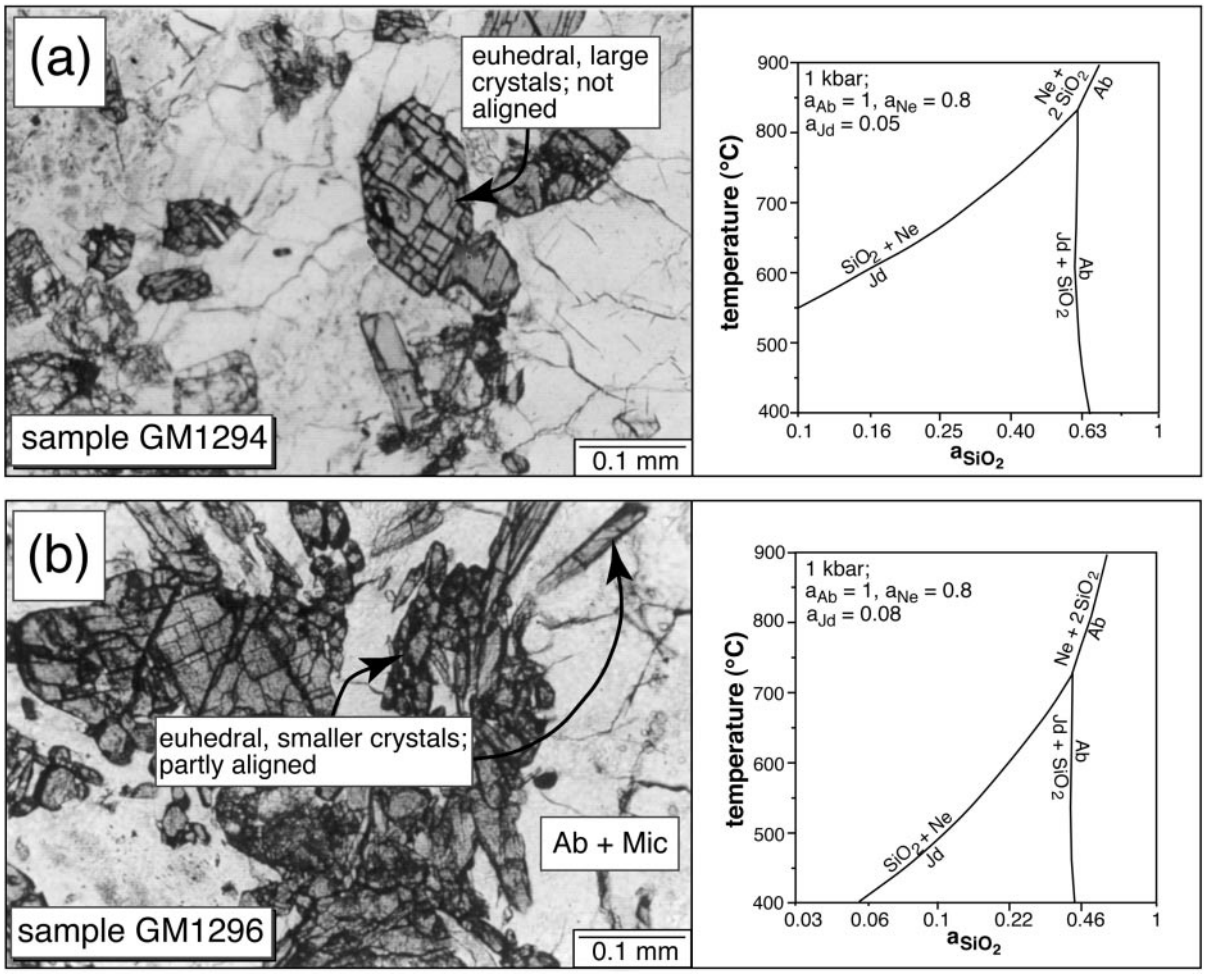

Fig. 6.

of excess silica [i.e. recording the highest temperatures (Hamilton, 1964), see Fig. 10].

For the late-magmatic assemblages, analcime-involving equilibria such as

$$3\ \mathrm{Anl} + 2\ \mathrm{NaCl} = \mathrm{Sod} + 3\ \mathrm{SiO_2} + 3\ \mathrm{H_2O} \quad (5)$$

or

$$\mathrm{Anl} + \mathrm{SiO_2} = \mathrm{Ab} + \mathrm{H_2O} \quad (6)$$

were used. In these calculations analcime was treated as a pure phase. SiO_2 unit activity was referred to a standard state of a pure SiO_2 modification at P and T; H_2O and NaCl unit activities refer to pure water and halite at P and T.

In principle, clinopyroxene–olivine–Fe–Ti oxide equilibria and equilibria involving Na–Al silicates provide information on solidus and liquidus conditions, respectively. The former depend on fast-diffusing cations such as Fe and Mg and involve minerals known to re-equilibrate and exsolve during cooling. The latter, in contrast, can be assumed to behave as a closed system after their formation—even in the presence of a melt—as re-equilibration would involve coupled substitutions and reconfiguration of the crystal structure after re-equilibration. This is unlikely to happen and therefore these equilibria are believed to be robust and to reflect early magmatic conditions or, more precisely, conditions during formation of the last mineral in a specific assemblage, whereas the Fe–Mg-involving equilibria probably reflect last mutual contact with a melt and hence approach solidus conditions.

In some augite syenite samples, the primary magmatic nepheline is replaced by a mixture of hydrogrossular, analcime, sodalite and muscovite that is in mutual contact with both K-feldspar and plagioclase. In conjunction with the sodalite–nepheline–NaCl reaction (4), the reactions

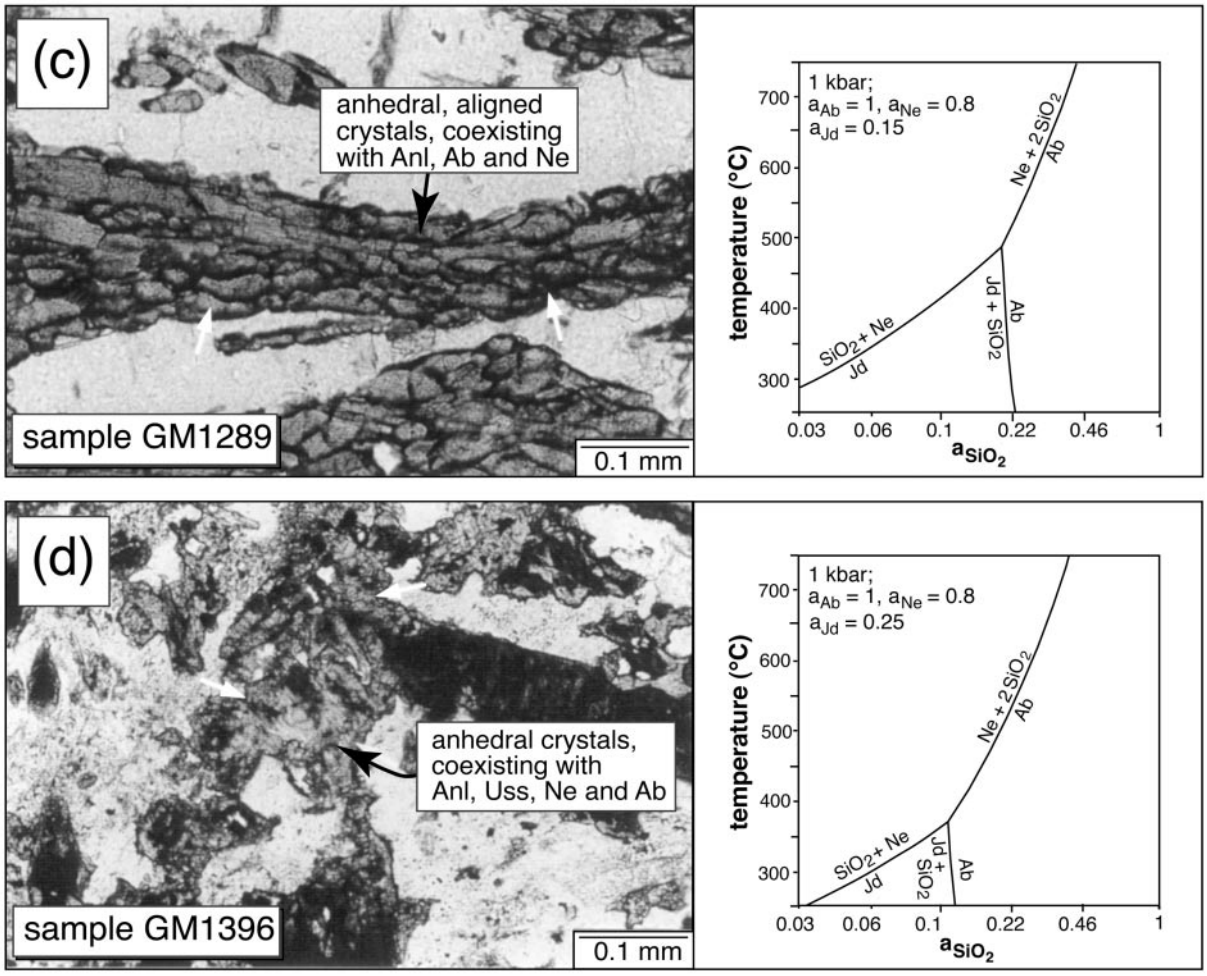

Fig. 6. (a)–(d) Textures and corresponding phase diagrams in lujavrites relating various textures to various conditions of formation. (See text for discussion.)

$$4\ \text{Kfsp} + \text{Ne} + 4\ \text{Anl} + 6\ \text{An} = 2\ \text{Hgrs} + 5\ \text{Ab} + 4\ \text{Ms} \quad (7)$$

and

$$24\ \text{Kfsp} + 24\ \text{Anl} + 36\ \text{An} + \text{Sod} = 12\ \text{Hgrs} + 30\ \text{Ab} + 24\ \text{Ms} + 2\ \text{NaCl} \quad (8)$$

can be used to estimate temperature and minimum NaCl activity during this post-magmatic event. K-feldspar and plagioclase activities were calculated after Fuhrman & Lindsley (1988); end-member grossular was used in the calculations as a proxy for the almost pure hydrogrossular end member found in the samples, muscovite activity was calculated using an ideal site mixing model; sodalite and analcime were regarded having unit activities and a range of nepheline activities reflecting the measured range of nepheline compositions were used in the calculations.

Oxygen fugacity in the augite syenite was estimated by Larsen (1976) and by Marks & Markl (2001) based on Fe–Ti oxide stability. In the agpaitic rocks, the reaction

$$18\ \text{Arf} + 11\ \text{O}_2 = 38\ \text{Aeg} + 4\ \text{Aen} + 18\ \text{H}_2\text{O} + 20\ \text{SiO}_2 \quad (9)$$

can, in principle, be used to estimate oxygen fugacity in rocks with an amphibole–clinopyroxene–aenigmatite assemblage. No thermodynamic data exist for these phases, but the experiments of Ernst (1962) allow an approximation of the above equilibrium in the Mg- and Al-free system. Ernst's results were obtained in a quartz- and water-saturated system, but we corrected them for reduced SiO_2 and H_2O activities by graphically estimating a log K value from his figures.

Equilibria involving olivine, clinopyroxene and Fe–Ti oxides were calculated using QUILF (Andersen *et al.*, 1993), whereas all other calculations used the GEOCALC

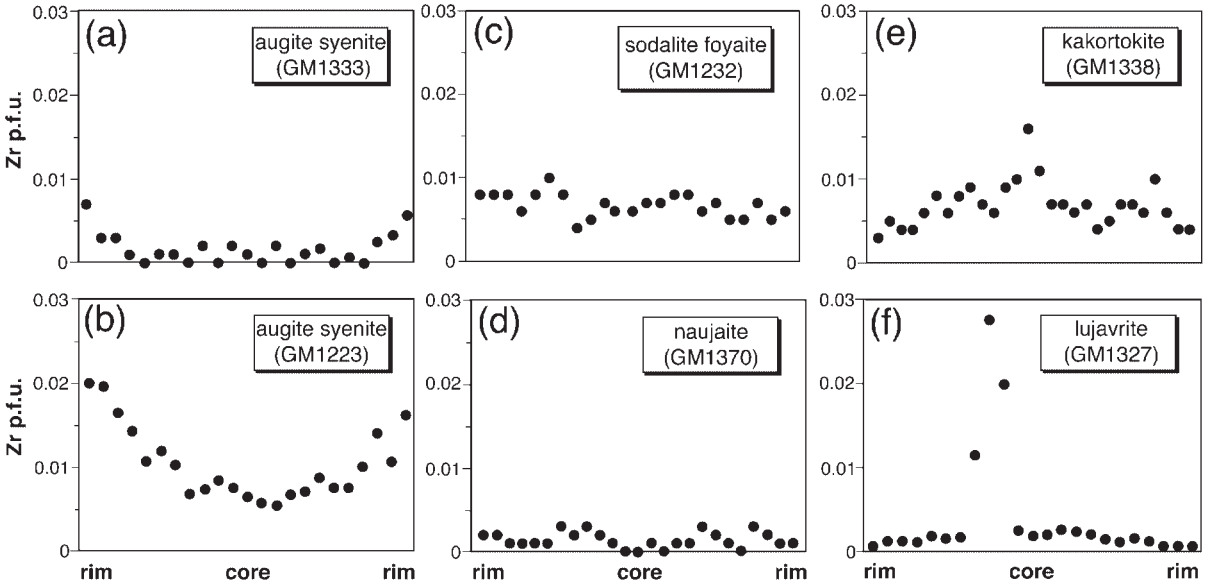

Fig. 7. Zr contents of zoned pyroxene crystals in the various rock types: (a) and (b) augite syenite; (c) sodalite foyaite; (d) naujaite; (e) kakortokite; (f) lujavrite. Profile widths are 2·5 mm, 2·0 mm, 1·5 mm, 2·0 mm, 0·6 mm and 0·1 mm, respectively.

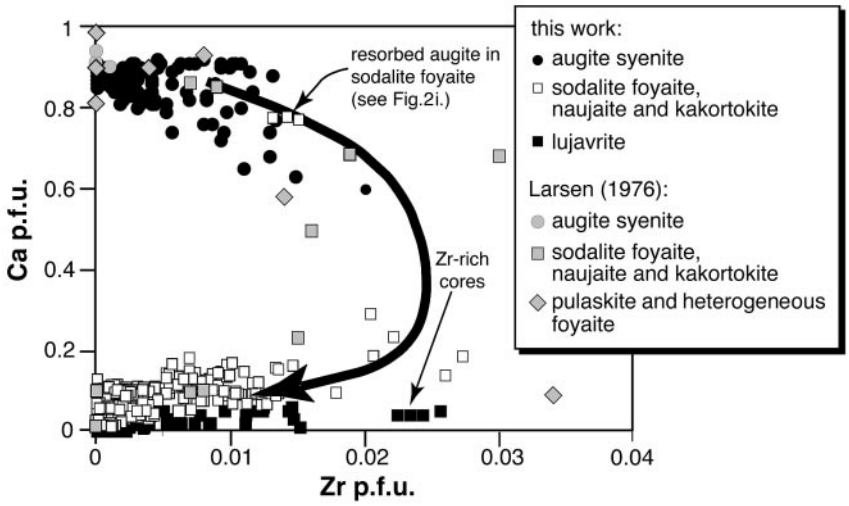

Fig. 8. Ca vs Zr in Ilímaussaq pyroxenes. (Note the early increase and later decrease of Zr during fractionation.) The black arrow shows the fractionation trend. Also shown are published pyroxene analyses from Ilímaussaq according to Larsen (1976).

software of Berman *et al.* (1987) and Lieberman & Petrakakis (1990) with the database of Berman (1988). Thermodynamic data for sodalite, NaCl, analcime and nepheline, however, were inserted into this database, and were taken from Sharp *et al.* (1989; nepheline, NaCl and sodalite) and from the SUPCRT92 database (Johnson *et al.*, 1992; analcime). Where feasible, only data from one source were used in one set of calculations to assure internal consistency.

CHANGES IN THE INTENSIVE PARAMETERS DURING CRYSTALLIZATION

Pressure

Pressure was set at 1 kbar in all calculations, for the following reasons:

(1) fluid inclusions in the alkali granite (Konnerup-Madsen & Rose-Hansen, 1984) and in the lujavrite

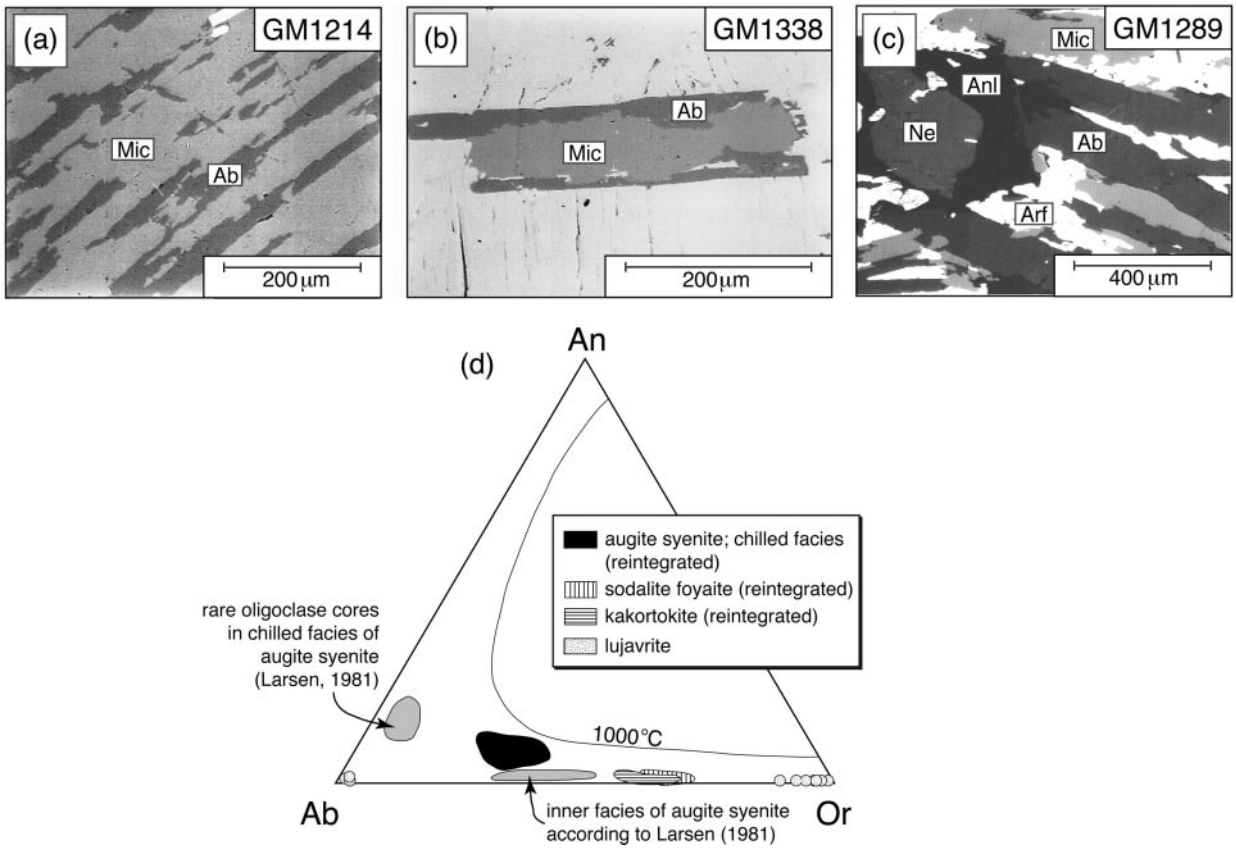

Fig. 9. Different exsolution textures of feldspar observed in (a) augite syenite and sodalite foyaite and (b) in kakortokite. These images were used to reintegrate magmatic feldspar compositions shown in the feldspar ternary An–Ab–Or (d). For comparison, feldspar analyses from Larsen (1981) are added. The 1000°C isotherm is after Fuhrman & Lindsley (1988). In lujavrites two separate feldspars (albite and microcline) crystallized (c).

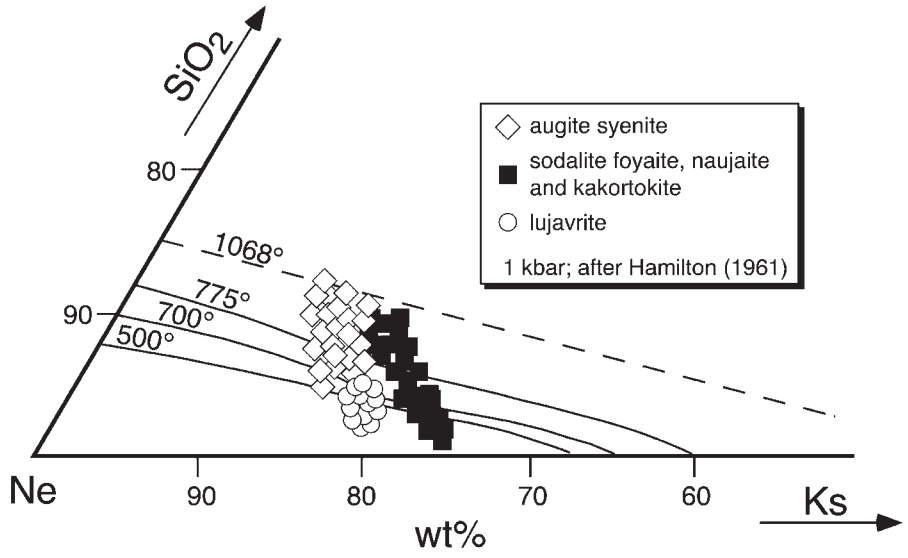

Fig. 10. Ne–Ks–SiO_2 triangle showing the nepheline compositions from Ilímaussaq rocks. Liquidus lines are after Hamilton (1961).

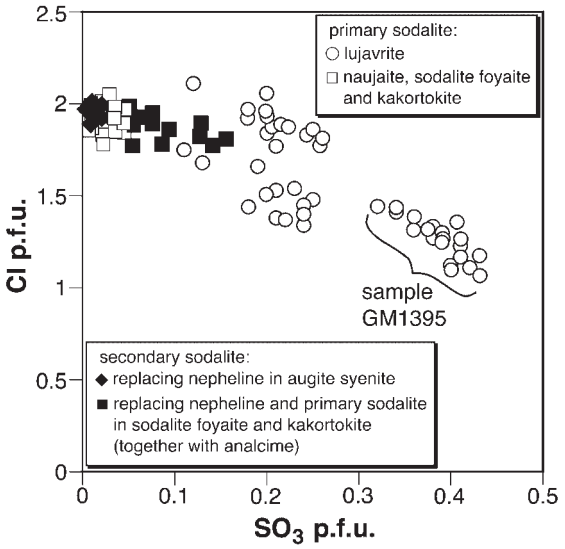

Fig. 11. Chlorine vs SO_3 plot for Ilímaussaq sodalite.

(Sommer, 1999) are consistent with a pressure of formation of ~1 kbar;

(2) the overburden of the Eriksfjord formation on top of Ilímaussaq was estimated to ~3–4 km, corresponding again to a pressure of ~1 kbar within the intrusion (Konnerup-Madsen & Rose-Hansen, 1984);

(3) the various melts are assumed to have crystallized and/or equilibrated (if they brought phenocrysts with them) all at the same level.

It is only in some naujaite samples that complications arise. As shown in Fig. 12, primary fluid inclusions in sodalite crystals in various naujaite samples crystallized at magmatic temperatures between 700 and 900°C at pressures between 1·5 and 3·5 kbar. Secondary methane-bearing inclusions along cracks indicate pressures of 1–1·5 kbar at temperatures of 500–700°C. The secondary inclusions are interpreted to reflect cracking of the phenocrysts during final emplacement. Aqueous inclusions in naujaite indicate ~1 kbar at 400°C (for derivation of the various temperature estimates see below). We interpret this to result from sodalite crystallization within a rising magma emplaced and solidified at ~1 kbar. This interpretation is consistent with the textural interpretation that sodalite is an early liquidus phase and that the naujaite is a sodalite flotation cumulate (Ferguson, 1964).

Temperature and silica activity

Information on temperature and silica activity of most Ilímaussaq rock types is compiled in Figs 9, 10, 13 and 14. Nepheline liquidus thermometry after Hamilton (1964) reveals significant differences among the various sample groups, although the spread in calculated temperatures is large (Fig. 10). Some analyses from the augite syenite plot on the 1068°C isotherm whereas the nepheline analyses lowest in SiO_2 indicate temperatures as low as 500°C. The highest temperatures recorded by nepheline in a single rock type are regarded as liquidus or at least closest to liquidus temperatures and are broadly consistent with other temperature estimates. Accordingly, nepheline compositions indicate liquidus temperatures in excess of 1000°C in the nepheline-bearing portions of the augite syenite, slightly lower temperatures as high as 950°C in sodalite foyaite, kakortokite and naujaite, and liquidus temperatures of ~750°C in lujavrite.

On the basis of feldspar compositions (Fig. 9), liquidus temperatures of the augite syenite were in excess of 950°C, whereas solidus temperatures deduced from mafic mineral equilibria reached as low as ~600°C. Silica activity in these rocks decreases during fractional crystallization mainly of alkali feldspars from values of ~0·8 or even unity (in rare cases where presumably sandstone contamination produced a quartz-saturated assemblage) to values of ~0·4. These estimates were derived from QUILF calculations (Andersen *et al.*, 1993) as well as from Ab–Jd–Ne equilibria. They are reported in detail by Marks & Markl (2001) and compiled in Fig. 13.

Equilibria among Ne, Ab and Jd (components in early magmatic nepheline solid solution, alkali feldspar and clinopyroxene) provide the only means to estimate temperatures or silica activities in the sodalite foyaite, naujaite and kakortokite (Fig. 14a–d). Equilibration temperatures between 800 and 700°C occur at SiO_2 activities between 0·3 and 0·5. Late-stage aegirine rims around magmatic amphiboles (Fig. 14b) indicate temperatures of ~550°C at silica activities around 0·25.

In the lujavrites, the texturally different types of clinopyroxene (Fig. 6a–d) record temperatures between ~800°C and 350°C. Pyroxenes indicating temperatures of ~450–500°C are found in textures that reflect solidus conditions (Fig. 6c), whereas the lowest temperatures are derived from pyroxenes that have probably grown during hydrothermal alteration (Fig. 6d). Silica activity drops from values of ~0·6 at 800°C to ~0·15 at 350°C; these values reflect magmatic and hydrothermal conditions, respectively.

The hydrothermal sodalite–hydrogrossular–analcime assemblage in some augite syenite samples (Fig. 2c and 2d) records ~400°C at a fixed silica activity of ~0·1 if calculated with the whole variation of mineral chemistry observed (Fig. 15a). In summary, the Ilímaussaq nepheline syenites record a crystallization interval between ~1000 and ~450–500°C. During fractional crystallization and subsequent hydrothermal activity, the silica activity continuously decreases from 0·8 to ~0·1.

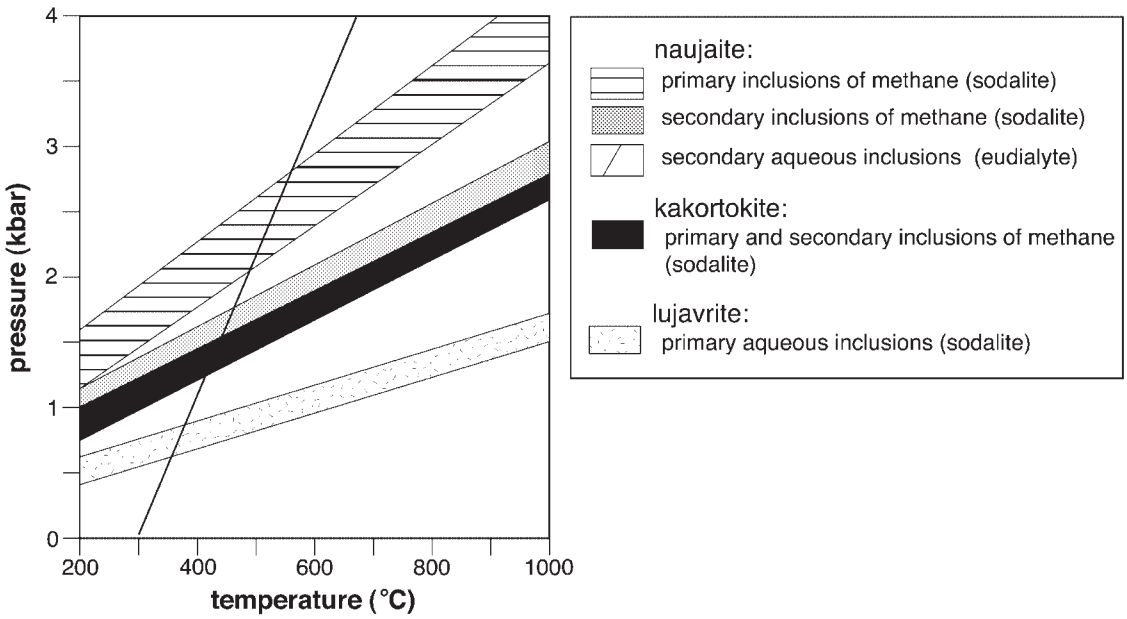

Fig. 12. *P–T* diagram for fluid inclusion data from various Ilímaussaq rock types. Data are from Schwinn (1999) and Sommer (1999) and will be presented in detail elsewhere. (For interpretation, see text.)

NaCl and water activity

NaCl activity can be calculated from both phase equilibria and fluid inclusion freezing point depression data. Sodalite–nepheline equilibrium buffers NaCl activity in almost the whole course of agpaite crystallization (sodalite is absent in relatively few kakortokite and lujavrite samples only). On the basis of this equilibrium, NaCl activity drops strongly during fractionation. For early magmatic temperatures of ~800°C, phase equilibria among nepheline and sodalite reveal NaCl activities of ~0·3–0·4, whereas NaCl activities between 0·01 and 0·1 are indicated for late-magmatic temperatures in all agpaitic rocks (Fig. 15b and c). In support of this, primary and secondary aqueous inclusions in lujavrites as detailed above show salinities in the 3 wt % NaCl equivalent range corresponding to NaCl activities of ~0·01 if an

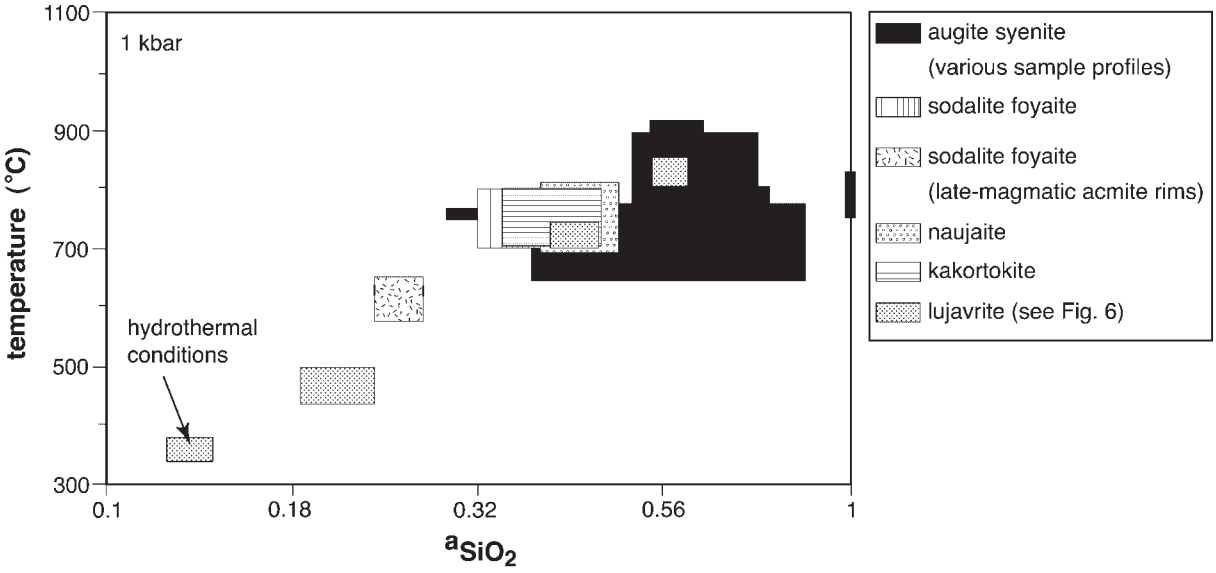

Fig. 13. Temperature–silica activity diagram showing the estimates for all rock types derived from QUILF calculations (Andersen *et al.*, 1993) as well as from Ab–Jd–Ne equilibria.

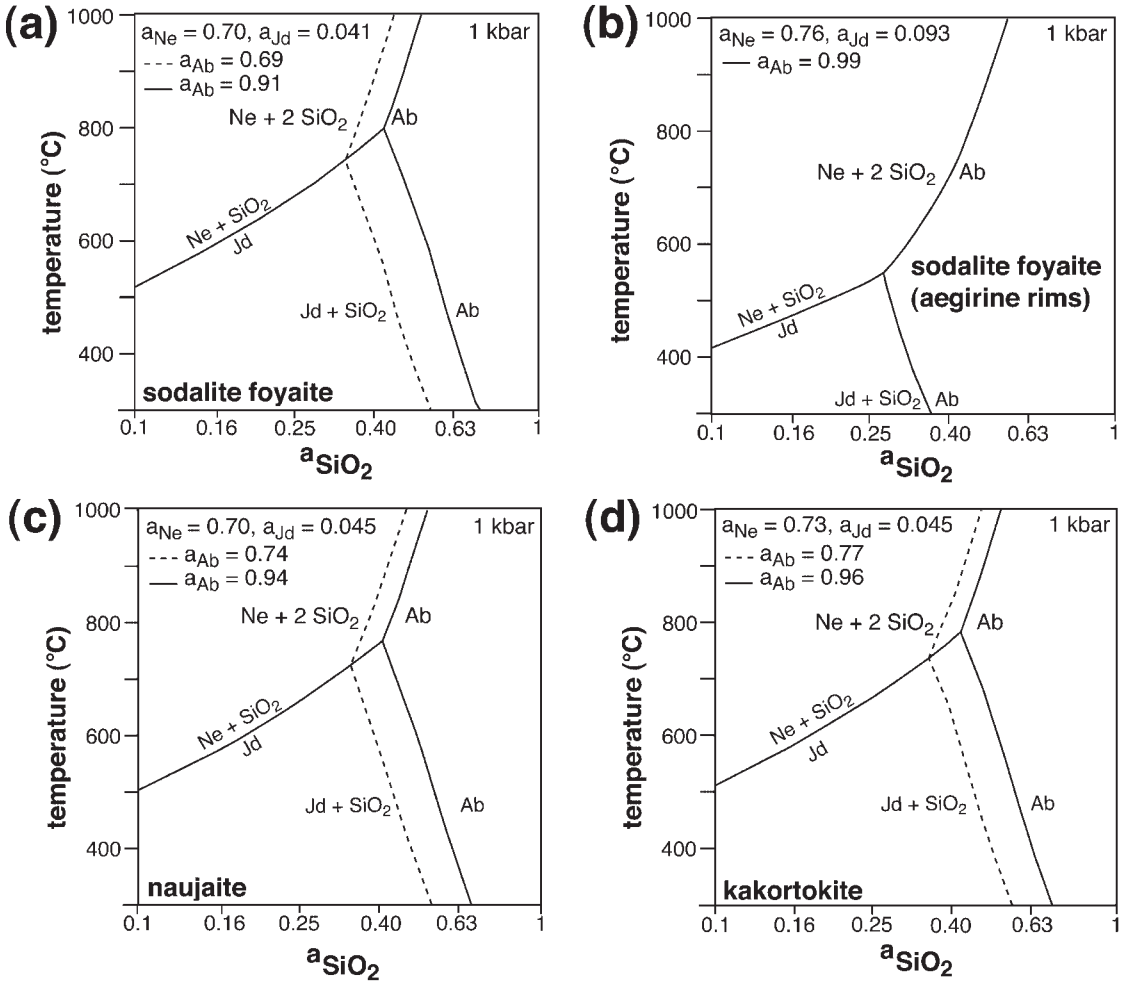

Fig. 14. Temperature–silica activity diagrams showing equilibria among Ab, Ne and Jd for the agpaitic rocks of Ilímaussaq, except for the lujavrites, which are shown in Fig. 6. The activity of Ne was calculated from the Ne analysis corresponding to the highest temperature (see Fig. 10), the activity of jadeite in (a), (c) and (d) was calculated from the Jd-richest analysis of texturally early clinopyroxene, in (b) of texturally late aegirine, and the two activities of Ab correspond to the highest and lowest Ab contents in alkali feldspars of the respective rock type.

ideal solution model is used. Because the hydrogrossular–analcime–sodalite assemblage in the augite syenite is consistent with these low salinities, NaCl activities drop from ~0·4 to ~0·01 in the course of crystallization and post-magmatic hydrothermal activity.

Maximum water activities were estimated for the augite syenite from the equilibrium

$$2\ \text{Kfsp} + 3\ \text{Fa} + 2\ \text{H}_2\text{O} = 2\ \text{Ann} + 3\ \text{SiO}_2 \quad (10)$$

for the silica activities calculated above (Fig. 16). Late-magmatic biotite was assumed to have formed between 600 and 700°C to estimate maximum water activities in this stage. Using an ideal site mixing model for the biotite and the fayalite (two site mixing) and the Fuhrman & Lindsley (1988) model for feldspar, extremely low water activities of ~0·2 were calculated (Fig. 16). The absence of biotite in the early crystallization stages is interpreted to reflect even lower water activities. In constrast, the late-stage agpaitic analcime assemblages indicate water activities between 0·7 and unity at 400°C in the augite syenite (Fig. 17a), between 0·4 and 0·8 at 500°C in the sodalite foyaite, naujaite and kakortokite (Fig. 17b), and around unity at 500°C in the lujavrites (Fig. 17c). These results are in agreement with fluid inclusion data. Hence, contrary to NaCl activity, water activity significantly increases during fractionation.

Oxygen fugacity

Relative oxygen fugacities in the augite syenite decrease during fractional crystallization from about FMQ (fayalite–magnetite–quartz) – 1 to FMQ – 2, to below FMQ – 4, reaching in some samples the calculated stability of

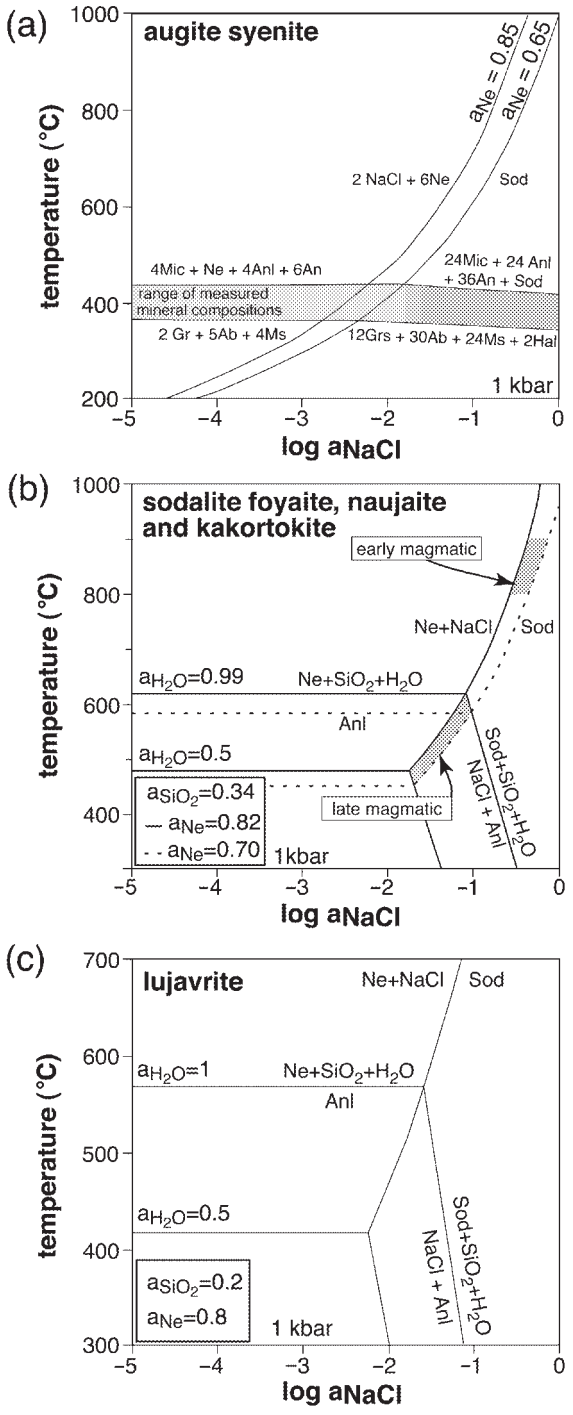

Fig. 15. Temperature–log a_{NaCl} diagrams showing phase equilibria used to estimate NaCl activity in augite syenite (a) and the agpaitic rocks (b and c). In augite syenite (a), the range of measured mineral compositions was used, resulting in a broad band rather than a single reaction line.

native iron, which was, however, not observed in any sample (Marks & Markl, 2001).

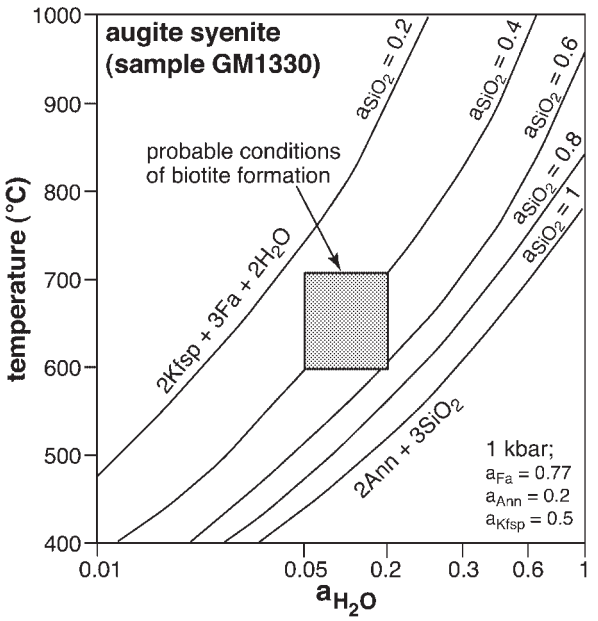

Fig. 16. Temperature–a_{H_2O} diagram for estimation of magmatic water activity in the augite syenite.

The agpaitic rocks lack both Fe–Ti-oxides and quartz, but the occurrence of arfvedsonitic amphibole, aegirine pyroxene and aenigmatite or olivine allows us to constrain the oxygen fugacity (see also Larsen, 1977) by reactions such as reaction (9). After steady decrease of f_{O_2} in the augite syenite stage, oxygen fugacity rises approximately on or parallel to the 'Arf–Acm' buffer curve in Fig. 18, which represents the approximate, activity-corrected curve where arfvedsonite and aegirine coexist according to the experiments of Ernst (1962). A part of it is represented by reaction (9). The bold black curve in Fig. 18 is meant to represent combined deep-level (at high temperatures) and high-level (at lower temperatures) fractionation, and the grey curve labelled augite syenite refers to high-level fractionation only. Augite syenite and agpaitic rocks show different, but mostly subparallel evolution trends. As shown by the remarks at the top of Fig. 18, f_{O_2} may be buffered by various solid-phase buffers or may not be buffered at all during the various stages of crystallization. Oxygen fugacity buffered by aegirine–arfvedsonite–aenigmatite assemblages increases during fractionation and cooling, probably to values of FMQ + 2 to FMQ + 4; this is close to or equal to the magnetite–haematite buffer (Fig. 18). After aenigmatite is no longer a liquidus phase, i.e. in the lujavrites, oxygen fugacity is no longer constrained by a solid–solid buffer reaction and f_{O_2} can, in principle, increase or decrease. The transition from a methane-dominated to an aqueous fluid in the late lujavrite crystallization stages appears to

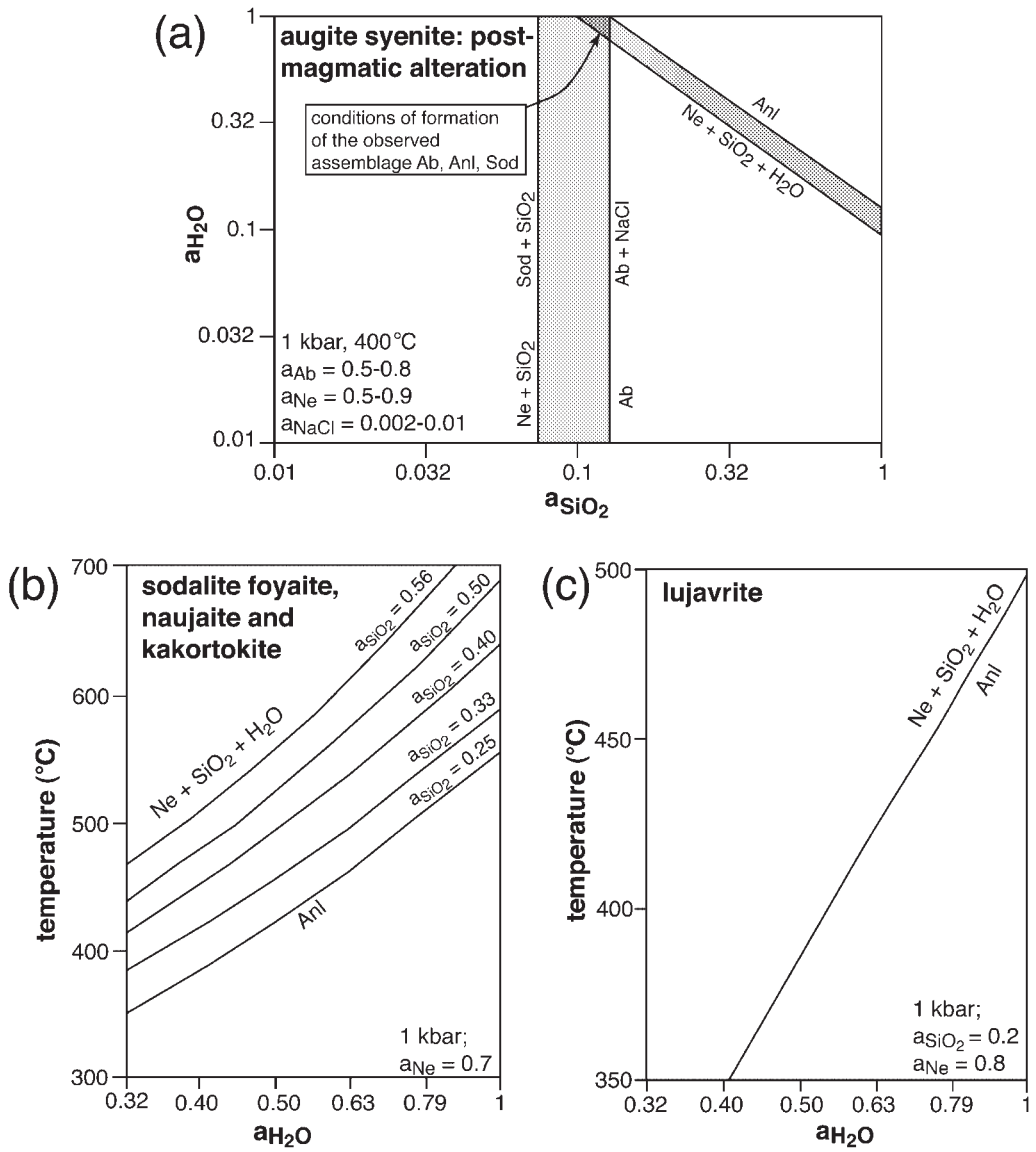

Fig. 17. (a) a_{H_2O}–a_{SiO_2} and (b, c) temperature–a_{H_2O} diagrams with equilibria in the system Na–Al–Si–O–H–Cl used to calculate post-magmatic water activity in the various rock types: (a) for augite syenite; (b) for foyaite, naujaite and kakortokite; (c) for lujavrite.

occur at oxygen fugacities close to the magnetite–haematite buffer (Fig. 18).

DISCUSSION

The above calculations will be discussed based on the genetic model of Larsen & Sørensen (1987), which assumes fractionation at depth (crust–mantle boundary?) of the melts parental to the Ilímaussaq rocks. Successive 'leaking' of this deep-level magma chamber is responsible for the three magma batches rising to the high-level chamber, where further low-pressure fractionation continues. The calculations and observations reported above reveal the following important points:

(1) the earliest augite syenite melt at Ilímaussaq was reduced (FMQ – 1 to FMQ – 2), had methane as a stable fluid phase, very low water activities (<0·2), relatively low silica activities (~0·8) and relatively high alkali/Al ratios [~0·9 based on whole-rock analyses by Engell (1973); 0·83 after Bailey *et al.* (2001)].

(2) High-level fractionation of augite syenitic melts leads to drastically reduced SiO_2 activities down to ~0·4 and strong reduction down to FMQ – 4 and below (Marks & Markl, 2001).

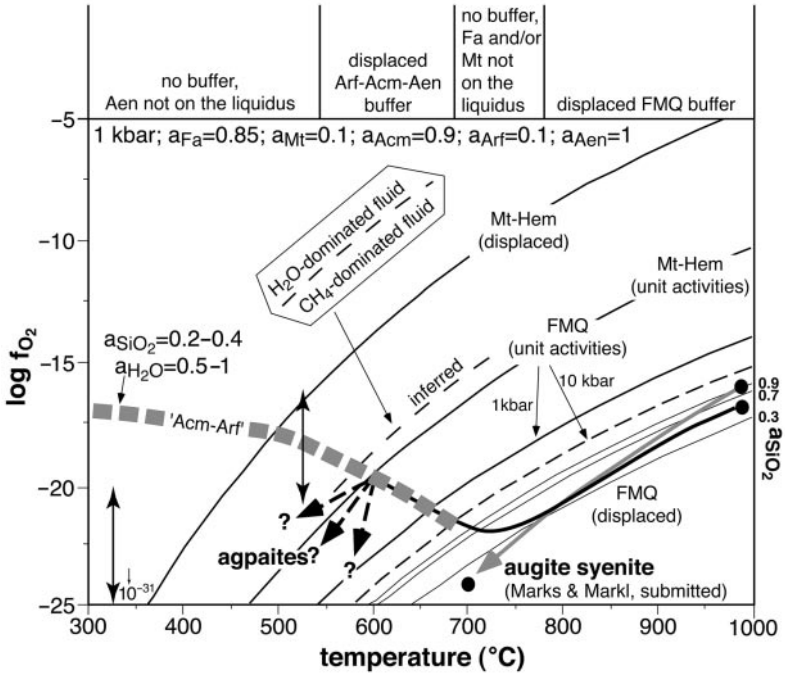

Fig. 18. Temperature–log f_{O_2} plot illustrating the evolution of oxygen fugacity during fractionation of the Ilímaussaq melts. 'Acm–Arf' is the approximate position of various equilibria along which aegirine and arfvedsonite stably coexist. FMQ, fayalite–magnetite–quartz buffer; Mt, magnetite; Hem, haematite; Aen, aenigmatite. The bold black curve represents combined deep-level (at high temperatures) and high-level (at lower temperatures) fractionation (see Marks & Markl, 2001); the grey curve labelled augite syenite refers to high-level fractionation only. The notes at the top of the figure indicate if and how f_{O_2} is buffered in the various crystallization stages. Double arrows are oxygen fugacity estimates derived from ore mineral stabilities (Karup-Møller, 1978).

(3) At the same time, deep-level fractionation also leads to decreasing SiO_2 activities and increasing (Na + K)/Al ratios (however, much more slowly than during high-level fractionation, as a result of the much larger magma reservoir involved) thereby giving rise to the highly alkaline and finally agpaitic rocks in the next syenitic magma batch. Increasing alkali/Al ratios require that plagioclase or spinel has to fractionate until the alkali/Al ratio exceeds unity. The anorthosite xenoliths found all over the Gardar province may be the witness of such deep-seated processes. After this state is reached, crystallization of alkali feldspar and nepheline further increases the alkali/Al ratio (it should be noted that crystallizing a Na:Al = 1:1 phase such as albite from a melt with Na/Al value >1 increases Na/Al further). Methane is still the stable fluid phase, but f_{O_2} rises significantly, to values of FMQ + 2 and above, whereas silica activity drops to values of 0·3 in the late stages of the last, peralkaline magma batch and NaCl activity in the melt is high (of the order of 0·3–0·4), leading to crystallization of sodalite.

(4) The kakortokite–lujavrite magma batch starts with similar silica activities of the order of 0·4. In the latest stages of lujavrite crystallization and in the hydrothermal stage, an aqueous fluid with very low salinity is exsolved and silica activity drops to values <0·2. Analcime becomes stable, indicating that H_2O activity has risen to values between 0·7 and unity, and NaCl activity has dropped drastically to values <0·1, probably as a result of consumption of Cl by sodalite crystallization.

Even though the data are approximations only, they reveal the general trends and allow us to quantify the changes of various parameters during crystallization of the Ilímaussaq melts. The more or less continuous trends in parameters such as the activity of SiO_2, NaCl and H_2O activity support the Larsen & Sørensen (1987) model insofar as it seems reasonable to interpret the various intrusive events seen in the field as various, successive batches of one continuously fractionating magma at depth. The systematically falling temperature where the most evolved assemblages of one batch record lower temperatures than the earliest assemblages of the successive batch are also in agreement with this model.

The new data serve to elaborate the model. The fact that in the final lujavrite stage most Fe in the rock is in its trivalent state and the coexistence of an aqueous fluid phase argue for relatively oxidized conditions around and above the magnetite–haematite buffer in these very late-stage melts. It is important to distinguish between the changes in the absolute values of f_{O_2} in bars and

between the changes relative to a solid-phase buffer such as FMQ. Depending on temperature and the phases crystallizing, the absolute value of f_{O_2} may change whereas the oxidation state of the system relative to FMQ stays the same. Karup-Møller (1978) showed in an extremely detailed and thorough investigation on the ore minerals present in the Ilímaussaq rocks that oxygen fugacities in the lujavrites and pegmatites were between 10^{-16} and 10^{-21} at ~500°C (see Fig. 18). In these conditions, native lead is stable and one would normally term it 'reduced'. However, these oxygen fugacities are still ~3–7 log units above the FMQ buffer and ~1–4 log units above the magnetite–haematite buffer at these conditions and can therefore be termed 'oxidized'—the iron is present in the trivalent state. We chose to solve this semantic problem by relating redox processes to the FMQ buffer only, and naming conditions of higher oxygen fugacity than this buffer 'oxidized' and conditions of lower oxygen fugacity 'reduced'.

The experimental equilibria among aegirine, arfvedsonite and aenigmatite of Ernst (1962) allow broad estimates of absolute f_{O_2} and, more importantly, of f_{O_2} evolution. If a reaction such as

$$5\ \mathrm{Aeg} + \mathrm{H_2O} = \mathrm{Arf} + 1{\cdot}5\ \mathrm{O_2} + \mathrm{Na_2O^{liquid}} + 2\ \mathrm{SiO_2^{liquid}} \quad (11)$$

or reaction (9) is responsible for the aegirine–arfvedsonite stability relationship, then decreasing silica activity would mean increasing f_{O_2}. If, however, the reaction

$$2\ \mathrm{Aeg} + \mathrm{H_2O} + \mathrm{FeO^{liquid}} + 2\ \mathrm{SiO_2^{liquid}} = \mathrm{Arf} + 0{\cdot}5\ \mathrm{O_2} \quad (12)$$

is important, then decreasing silica activity would lead to decreasing oxygen fugacity. The former appears to be the case in Ilímaussaq, as reaction (9) is a good proxy for many of the agpaitic rocks.

In the FMQ buffer reaction, decreasing silica activity also decreases the oxygen fugacity of this buffer assemblage or will lead to total consumption of fayalite. An increase in the alkali/Al ratio will lead to consumption of magnetite as a result of formation of aenigmatite or because of a reaction such as

$$\mathrm{mag} + 1{\cdot}5\ \mathrm{Na_2O^{liquid}} + 6\ \mathrm{SiO_2^{liquid}} + 0{\cdot}25\ \mathrm{O_2} = 3\ \mathrm{Aeg}. \quad (13)$$

In combination, this process leads to consumption and replacement of the characteristic augite syenite by the characteristic peralkaline assemblage. In Ilímaussaq, this occurred between the augite syenite and the foyaite–naujaite stage as evidenced by the scarcity or lack of Fe–Ti oxides in the Ilímaussaq peralkaline rocks. As soon as fayalite is consumed, the aegirine–arfvedsonite equilibrium will buffer f_{O_2} of the melt and this equilibrium in turn depends mainly on the water activity in the melt via, for example, the reaction

$$5\ \mathrm{Aeg} + \mathrm{H_2O} = \mathrm{Arf} + 1{\cdot}5\ \mathrm{O_2} + \mathrm{Na_2O^{liquid}} + 2\ \mathrm{SiO_2^{liquid}}. \quad (14)$$

It appears that in the augite syenite stage, the displaced FMQ reaction buffered f_{O_2}, whereas after the augite syenite stage, a_{H_2O} determined f_{O_2} via a solid-phase equilibrium such as reaction (14). In this case, f_{O_2} increases as a consequence of increasing a_{H_2O} and it was shown above that a_{H_2O} increases during fractionation. As the absolute value of f_{O_2} of the FMQ buffer reaction decreases with falling temperature, increasing f_{O_2} during fractionation would mean oxidation of the system also relative to FMQ (Fig. 18). By virtue of changing solid-phase buffers, alkaline and peralkaline melts of the agpaitic trend are deeply reduced in the early stages of crystallization, but highly oxidized in at least many of the late stages. The governing variables are silica and water activity.

SUMMARY AND CONCLUSIONS

The results of this study allow us to quantify the changes in physico-chemical parameters during crystallization of the syenitic rocks in the Ilímaussaq intrusive complex, South Greenland. The results support the model that a deep-seated magma chamber fractionated and successively released melt batches from its top. The melt batches rose to the present position of the Ilímaussaq complex, where they continued to fractionate in a closed system. Fluid inclusion data of the naujaite indicate that crystallization at least of sodalite started at ~10 km depth and continued during ascent of the melt. On the basis of the field observations [see Ferguson (1964) and later papers summarized by Bailey *et al.* (1981) and Sørensen (2001)], radiogenic isotope geochemistry (Stevenson *et al.*, 1997), and the phase equilibrium studies presented here and by Marks & Markl (2001), we consider the following criteria crucial in the evolution of the extremely differentiated agpaitic rocks:

(1) the parental melts have to have very low water activities (<0·2); this most important condition ensures that an aqueous fluid phase is exsolved very late in the crystallization history of the melts. Elements such as Cl preferably partitioning into such a fluid phase are kept and enriched in the silicate melt to unusually high concentrations. This results in NaCl activities up to 0·4 and in extensive crystallization of sodalite. It appears that Cl is a passive parameter during agpaite crystallization.

(2) Low water activities may be the reason for or the consequence of the low oxidation state of the parental melts (e.g. Ulmer *et al.*, 1998). The parental melts reflect the oxidation state of the mantle from which they were derived and hence, low-f_{O_2} asthenospheric mantle appears to be the source of the Ilímaussaq parental melts.

(3) The trend towards low SiO_2 activities seen in the augite syenite unit can directly be deduced from the Ne–Ks–SiO_2 phase diagram of Schairer (1950). It is therefore crucial that the parental melt has a composition below the feldspar tie-line in this diagram that corresponds to sufficiently low SiO_2 activities of the parental melt, probably <0·8. These low silica activities are typical of Ne-normative alkali basalts.

(4) Oxygen fugacity appears to be controlled by two solid–solid buffers, which in turn are controlled by liquid parameters: displaced FMQ in the just saturated to slightly undersaturated melts (augite syenite in Ilímaussaq) and aegirine–arfvedsonite–aenigmatite in most of the agpaitic rocks. The former depends on silica activity in the melt, the latter on silica activity and water activity, and hence these parameters determine f_{O_2} in alkaline rocks. This also explains the paradox of why f_{O_2} decreases during augite syenite fractionation but increases later: decreasing SiO_2 activity forces the oxygen fugacity to decrease in the augite syenite via the FMQ equilibrium, whereas decreasing a_{SiO_2} and increasing a_{H_2O} control the rise of f_{O_2} in the agpaitic rocks according to reactions (9) and (14).

(5) As long as the parental melt has an alkali/Al ratio below unity, extensive fractionation of plagioclase and/or spinel has to occur to increase this ratio, which allows crystallization of minerals such as aegirine, sodalite or villiaumite (NaF) besides nepheline and feldspar. Plagioclase crystallization is evidenced by the common occurrence of anorthosite xenoliths in the Gardar province and also in the Kvanefjeld area of the Ilímaussaq complex (Sørensen *et al.* 1969, 1974). In contrast to fractionation of spinel, crystallization of intermediate plagioclase also reduces silica activity in the melt with increasing fractionation provided that silica contents are low enough in the parental magma.

(6) As strongly Si-undersaturated melts are highly reactive with granitic wall-rocks, it appears to be of special importance that a structure exists that serves as conduit for several successive melt batches. Late melt batches of such a succession will be protected from direct contact with the host rocks because their precursor melts already line the conduit. In accordance with the isotopic data of Stevenson *et al.* (1997), the augite syenite and the alkali granite represent the early, more or less strongly contaminated members of such a succession whereas the later agpaitic rocks are less contaminated or even uncontaminated. Furthermore, intrusion into a high-level magma chamber lined by augite syenite effectively minimizes contact of the agpaitic melts with any host rock.

The scarcity of agpaitic rocks may be related to the scarcity of localities where such a mixture of chemical and physical conditions are realized.

ACKNOWLEDGEMENTS

We are grateful to H. Müller-Sigmund for her help with the microprobe. Discussions with E. Woermann and M. Westphal, and thoughtful and constructive reviews by J. C. Schumacher, an anonymous reviewer and especially by J. Bailey helped to improve the manuscript significantly. Financial funding for this work by the Deutsche Forschungsgemeinschaft (grant Ma2135-1/1) is gratefully acknowledged. This paper is Contribution to the Mineralogy of Ilímuassaq No. 113.

REFERENCES

Andersen, D. J., Lindsley, D. H. & Davidson, P. M. (1993). QUILF: a PASCAL program to assess equilibria among Fe–Mg–Mn–Ti oxides, pyroxenes, olivine, and quartz. *Computers and Geosciences* **19**, 1333–1350.

Bailey, J. C., Larsen, L. M. & Sørensen, H. (1981). The Ilímaussaq intrusion, South Greenland. A progress report on geology, mineralogy, geochemistry and economic geology. *Rapport Grønlands Geologiske Undersøgelse* **103**, 130 pp.

Bailey, J. C., Gwozdz, R., Rose-Hansen, J. & Sørensen, H. (2001). Geochemical overview of the Ilímaussaq alkaline complex, South Greenland. In: Sørensen, H. (ed.) *The Ilímaussaq Alkaline Complex. Bulletin Grønlands Geologiske Undersøgelse* (in press).

Berman, R. (1988). Internally consistent thermodynamic data for minerals in the system Na_2O–K_2O–CaO–MgO–FeO–Fe_2O_3–Al_2O_3–SiO_2–TiO_2–H_2O–CO_2. *Journal of Petrology* **29**, 445–522.

Berman, R. G., Brown, T. H. & Perkins, E. H. (1987). Geo-Calc; software for calculation and display *P–T–X* phase diagrams. *American Mineralogist* **72**, 861–862.

Blundell, D. J. (1978). A gravity survey across the Gardar Igneous Province, SW Greenland. *Journal of the Geological Society, London* **135**, 545–554.

Bridgwater, D. (1967). Feldspathic inclusions in the Gardar igneous rocks of South Greenland and their relevance to the formation of major anorthosites in the Canadian Shield. *Canadian Journal of Earth Sciences* **4**, 995–1014.

Bridgwater, D. & Harry, W. T. (1968). Anorthosite xenoliths and plagioclase megacrysts in Precambrian intrusions of South Greenland. *Meddelelser om Grønland* **185**(2), 243 pp.

Emeleus, C. H. (1964). The Grønnedal-Ika alkaline complex, South Greenland. The structure and geological history of the complex. *Meddelelser om Grønland* **172**(3), 75 pp.

Emeleus, C. H. & Upton, B. G. J. (1976). The Gardar period in southern Greenland. In: Escher, A. & Watt, W. S. (eds) *Geology of Greenland.* Copenhagen: Geological Survey of Greenland, pp. 152–181.

Engell, J. (1973). A closed system crystal-fractionation model for the agpaitic Ilímaussaq intrusion, South Greenland, with special reference to the lujavrites. *Bulletin of the Geological Society of Denmark* **22**, 334–362.

Ernst, W. G. (1962). Synthesis, stability relations, and occurrences of riebeckite and riebeckite–arfvedsonite solid solutions. *Journal of Geology* **70**(6), 689–736.

Ferguson, J. (1964). Geology of the Ilímaussaq alkaline intrusion, South Greenland. *Bulletin Grønlands Geologiske Undersøgelse* **39**, 82 pp.

Forsberg, R. & Rasmussen, K. L. (1978). Gravity and rock densities in the Ilímaussaq area, South Greenland. *Rapport Grønlands Geologiske Undersøgelse* **90**, 81–84.

Fuhrman, M. L. & Lindsley, D. H. (1988). Ternary-feldspar modeling and thermometry. *American Mineralogist* **73**, 201–205.

Gerassimovsky, V. I. & Kuznetsova, S. Y. (1967). On the petrochemistry of the Ilímaussaq intrusion, south Greenland. *Geochemistry International* **4**(2), 236–246.

Hamilton, D. L. (1964). Nephelines as crystallisation temperature indicators. *Journal of Geology* **69**, 321–329.

Holland, T. J. B. (1990). Activities of components in omphacitic solid solutions; an application of Landay theory of mixtures. *Contributions to Mineralogy and Petrology* **105**, 446–453.

Johnson, J. W., Oelkers, E. H. & Helgeson, H. (1992). SUPCRT92: a software package for calculating the standard molal thermodynamic properties of minerals, gases, aqueous species, and reactions from 1 to 5000 bars and 0 to 1000°C. *Computers and Geosciences* **18**, 899–947.

Jones, A. P. & Peckett, A. (1980). Zirconium-bearing aegirines from Motzfeldt, South Greenland. *Contributions to Mineralogy and Petrology* **75**, 251–255.

Karup-Møller, S. (1978). The ore minerals of the Ilímaussaq intrusion: their mode of occurrence and their conditions of formation. *Bulletin Grønlands Geologiske Undersøgelse* **127**, 51 pp.

Kogarko, L. N. (1974). Role of volatiles. In: Sørensen, H. (ed.) *The Alkaline Rocks*. London: John Wiley, pp. 474–487.

Kogarko, L. N. & Romanchev, B. P. (1977). Temperature, pressure, redox conditions, and mineral equilibria in agpaitic nepheline syenites and apatite–nepheline rocks. *Geochemistry International* **14**, 113–128.

Kogarko, L. N. & Romanchev, B. P. (1982). Phase equilibria in alkaline melts. *International Geology Review* **25**(5), 534–546.

Konnerup-Madsen, J. & Rose-Hansen, J. (1984). Composition and significance of fluid inclusions in the Ilímaussaq peralkaline granite, South Greenland. *Bulletin de Minéralogie* **107**(2), 317–326.

Konnerup-Madsen, J., Larsen, E. & Rose-Hansen, J. (1979). Hydrocarbon-rich fluid inclusions in minerals from the alkaline Ilímaussaq intrusion, South Greenland. *Bulletin de Minéralogie* **102**, 642–653.

Konnerup-Madsen, J., Dubessy, J. & Rose-Hansen, J. (1985). Combined Raman microprobe spectrometry and microthermometry of fluid inclusions in minerals from igneous rocks of the Gardar province (south Greenland). *Lithos* **18**, 271–280.

Konnerup-Madsen, J., Kreulen, R. & Rose-Hansen, J. (1988). Stable isotope characteristics of hydrocarbon gases in the alkaline Ilímaussaq complex, South Greenland. *Bulletin de Minéralogie* **111**, 567–576.

Larsen, L. M. (1976). Clinopyroxenes and coexisting mafic minerals from the alkaline Ilímaussaq intrusion, south Greenland. *Journal of Petrology* **17**(2), 258–290.

Larsen, L. M. (1977). Aenigmatites from the Ilímaussaq intrusion, south Greenland: chemistry and petrological implications. *Lithos* **10**, 257–270.

Larsen, L. M. (1981). Chemistry of feldspars in the Ilímaussaq augite syenite with additional data on some other minerals. *Rapport Grønlands Geologiske Undersøgelse* **103**, 31–37.

Larsen, L. M. & Sørensen, H. (1987). The Ilímaussaq intrusion—progressive crystallization and formation of layering in an agpaitic magma. In: Fitton, J. G. & Upton, B. G. J. (eds) *Alkaline Igneous Rocks. Geological Society, London, Special Publications* **30**, 473–488.

Lieberman, J. & Petrakakis, K. (1990). TWEEQU thermobarometry, analysis of uncertainties and applications to granulites from western Alaska. *Canadian Mineralogist* **29**, 857–887.

Lindsley, D. H. (1983). Pyroxene thermometry. *American Mineralogist* **68**, 477–493.

Markl, G. (2001). A new type of silicate liquid immiscibility in peralkaline nepheline syenites (lujavites) of the Ilimaussaq intrusion, South Greenland. *Contributions to Mineralogy and Petrology* **141**, 458–472.

Markl, G., Marks, M. & Wirth, R. (2001). The influence of T, a_{SiO_2}, f_{O_2} on exsolution textures in Fe–Mg olivine: an example from augite syenite of the Ilímaussaq Intrusion, South Greenland. *American Mineralogist* **86**, 36–46.

Marks, M. & Markl, G. (2001). Fractionation and assimilation processes in the alkaline augite syenite unit of the Ilímaussaq Intrusion, South Greenland, as deduced from phase equilibria. *Journal of Petrology* **42**, 1947–1969.

Parsons, I. (1972). Petrology of the Puklen syenite–alkali granite complex, Nunarssuit, South Greenland. *Meddelser om Grønland* **195**(3), 73 pp.

Parsons, I. (1981). The Klokken gabbro–syenite complex, south Greenland: quantitative interpretation of mineral chemistry. *Journal of Petrology* **22**(2), 233–260.

Petersilie, I. A. & Sørensen, H. (1970). Hydrocarbon gases and bituminous substances in rocks from the Ilímaussaq alkaline intrusion, South Greenland. *Lithos* **3**, 59–76.

Pouchou, J. L. & Pichoir, F. (1984). A new model for quantitative X-ray microanalysis. Part 1: applications to the analysis of homogeneous samples. *Recherche Aerospatiale* **3**, 13–38.

Poulsen, V. (1964). The sandstones of the Precambrian Eriksfjord Formation in South Greenland. *Rapport Grønlands Geologiske Undersøgelse* **2**, 16 pp.

Powell, M. (1978). The crystallisation history of the Igdlerfigssalik nepheline syenite intrusion, Greenland. *Lithos* **11**, 99–120.

Schairer, J. F. (1950). The alkali feldspar join in the system $NaAlSiO_4$–$KAlSiO_4$–SiO_2. *Journal of Geology* **58**(5), 512–517.

Schwinn, G. (1999). Kristallisationsgeschichte und Fluidentwicklung in agpaitischen Gesteinen der Ilímaussaq Intrusion, Südgrönland. Masters thesis, University of Freiburg, 159 pp.

Sharp, Z. D., Helffrich, G. R., Bohlen, S. R. & Essene, E. J. (1989). The stability of sodalite in the system $NaAlSiO_4$–NaCl. *Geochimica et Cosmochimica Acta* **53**, 1934–1954.

Shearer, C. K. & Larsen, L. M. (1994). Sector-zoned aegirine from the Ilímaussaq alkaline intrusion, South Greenland: implications for trace-element behavior in pyroxene. *American Mineralogist* **79**, 340–352.

Sommer, H. (1999). Kristallisationsgeschichte und Fluidentwicklung in Lujavriten der Ilímaussaq Intrusion in Grönland. Masters thesis, University of Freiburg, 111 pp.

Sørensen, H. (1997). The agpaitic rocks—an overview. *Mineralogical Magazine* **61**, 485–498.

Sørensen, H. (ed.) (2001). *The Ilímaussaq Alkaline Complex. Bulletin Grønlands Geologiske Undersøgelse* (in press).

Sørensen, H. & Larsen, L. M. (1987). Layering in the Ilímaussaq alkaline intrusion, South Greenland. In: Parsons, I. (ed.) *Origins of Igneous Layering*. Dordrecht: D. Reidel, pp. 1–28.

Sørensen, H., Hansen, J. & Bondesen, E. (1969). Preliminary account of the geology of the Kvanefjeld area of the Ilímaussaq intrusion, South Greenland. *Rapport Grønlands Geologiske Undersøgelse* **18**, 40 pp.

Sørensen, H., Rose-Hansen, J., Nielsen, B. L., Løvborg, L., Sørensen, E. & Lundgaard, T. (1974). The uranium deposit at Kvanefjeld, the Ilímaussaq intrusion, South Greenland. *Rapport Grønlands Geologiske Undersøgelse* **60**, 54 pp.

Stephenson, D. (1976). The South Qôroq Centre nepheline syenites, South Greenland. Petrology, felsic mineralogy and petrogenesis. *Bulletin Grønlands Geologiske Undersøgelse* **118**, 55 pp.

Stephenson, D. & Upton, B. G. J. (1982). Ferromagnesian silicates in a differentiated alkaline complex: Kungnât Fjeld, South Greenland. *Mineralogical Magazine* **46**, 283–300.

Stevenson, R., Upton, B. G. J. & Steenfelt, A. (1997). Crust–mantle interaction in the evolution of the Ilímaussaq Complex, South Greenland: Nd isotopic studies. *Lithos* **40**, 189–202.

Ulmer, G. C., Grandstaff, D. E., Woermann, E., Göbbels, M., Schönitz, M. & Woodland, A. B. (1998). The redox stability of moissanite (SiC) compared with metal-oxide buffers at 1773 K and at pressures up to 90 kbar. *Neues Jahrbuch für Mineralogie, Abhandlungen* **172**(2/3), 279–307.

Upton, B. G. J. & Emeleus, C. H. (1987). Mid-Proterozoic alkaline magmatism in southern Greenland: the Gardar province. In: Fitton, J. G. & Upton, B. G. J. (eds) *Alkaline Igneous Rocks. Geological Society, London, Special Publications* **30**, 449–471.

Upton, B. G. J. & Fitton, J. G. (1985). Gardar dykes north of the Igaliko syenite complex, southern Greenland. *Rapport Grønlands Geologiske Undersøgelse* **127**, 24 pp.

Upton, B. G. J., Stephenson, D. & Martin, A. R. (1985). The Tugtutôq older giant dyke complex: mineralogy and geochemistry of an alkali gabbro–augite-syenite–foyaite association in the Gardar Provine of South Greenland. *Mineralogical Magazine* **49**(354), 624–642.

Ussing, N. V. (1912). Geology of the country around Julianehaab, Greenland. *Meddelelser om Grønland* **38**, 426 pp.